Volume 53
Number 25
7 July 2024
Pages 10363-10756

Dalton Transactions

An international journal of inorganic chemistry

rsc.li/dalton

ISSN 1477-9226

ROYAL SOCIETY OF CHEMISTRY

PERSPECTIVE

Jiaji Zhang *et al.*

Review on synthetic approaches and PEC activity performance of bismuth binary and mixed-anion compounds for potential applications in marine engineering

Dalton Transactions

ROYAL SOCIETY OF CHEMISTRY

PERSPECTIVE

View Article Online
View Journal | View Issue

Cite this: *Dalton Trans.*, 2024, **53**, 10376

Review on synthetic approaches and PEC activity performance of bismuth binary and mixed-anion compounds for potential applications in marine engineering

Jiaji Zhang, [a,b,c,d,e] Bingchu Mei, [b] Huiyu Chen[b,c] and Zaichun Sun *[b,e]

Photoelectrochemical (PEC) technology in marine engineering holds significant importance due to its potential to address various challenges in the marine environment. Currently, PEC-type applications in marine engineering offer numerous benefits, including sustainable energy generation, water desalination and treatment, photodetection, and communication. Finding novel efficient photoresponse semiconductors is of great significance for the development of PEC-type techniques in the marine space. Bismuth-based semiconductor materials possess suitable and tunable bandgap structures, high carrier mobility, low toxicity, and strong oxidation capacity, which gives them great potential for PEC-type applications in marine engineering. In this paper, the structure and properties of bismuth binary and mixed-anion semiconductors have been reviewed. Meanwhile, the recent progress and synthetic approaches were discussed from the point of view of the application prospects. Finally, the issues and challenges of bismuth binary and mixed-anion semiconductors in PEC-type photodetection and hydrogen generation are analyzed. Thus, this perspective will not only stimulate the further investigation and application of bismuth binary and mixed-anion semiconductors in marine engineering but also help related practitioners understand the recent progress and potential applications of bismuth binary and mixed-anion compounds.

Received 24th April 2024,
Accepted 16th May 2024

DOI: 10.1039/d4dt01212g

rsc.li/dalton

1. General introduction

The photoelectrochemical (PEC) conversion process plays a significant role in various fields like marine engineering, owing to various advantages such as high efficiency, integration of renewable energy, grid stabilization, compact size, and environmental benefits.[1–3] The PEC process reaction involves the utilization of light energy to drive electrochemical processes at the surface between the photoelectrode and electrolyte (Fig. 1). Under the illumination of sunlight, PEC water splitting occurred on the surface of the photoelectrodes, offering a sustainable pathway for hydrogen production through the reduction of H^+.[4–6] Meanwhile, the PEC-type photodetectors have been regarded as a kind of self-powered photodetector with high photoresponsivity and a fast response speed, which can be used for underwater optical communication and display.[7] In addition, PEC-type devices can be used as sensors for the detection of heavy metal ions and degradation of pollutants.[8] Thus, embracing PEC technology can help establish a greener and more sustainable strategy for marine industries and coastal communities.

Since TiO_2 electrodes have been used for photoelectrochemical degradation and hydrogen production under ultraviolet light, the PEC-type technique has become a hot research area in academia and industry and attracted widespread attention.[9] However, due to its wide bandgap, TiO_2 can only utilize the ultraviolet portion of sunlight, resulting in a low energy conversion efficiency.[1–3,10–12] Finding suitable visible light-driven semiconductors has been regarded as one of the main research themes in PEC-type applications. Recently, bismuth-based semiconductors have received widespread attention due to their promising optical and electrical properties.[13–17] Bismuth (Bi) is a rare heavy metal element in nature with low toxicity and radioactivity, and can be called a "green

[a]*Sanya Science and Education Innovation Park, Wuhan University of Technology, Sanya 572025, China*
[b]*School of Materials Science and Engineering, Wuhan University of Technology, Wuhan 430070, China. E-mail: sun.zaichun@whut.edu.cn*
[c]*School of Civil Engineering and Architecture, Wuhan University of Technology, Wuhan 430070, China*
[d]*Birmingham Centre for Energy Storage & School of Chemical Engineering, University of Birmingham, Birmingham, B152TT, UK*
[e]*Hainan Yourui Cohesion Technology Co., Ltd, Sanya, 572025, China*

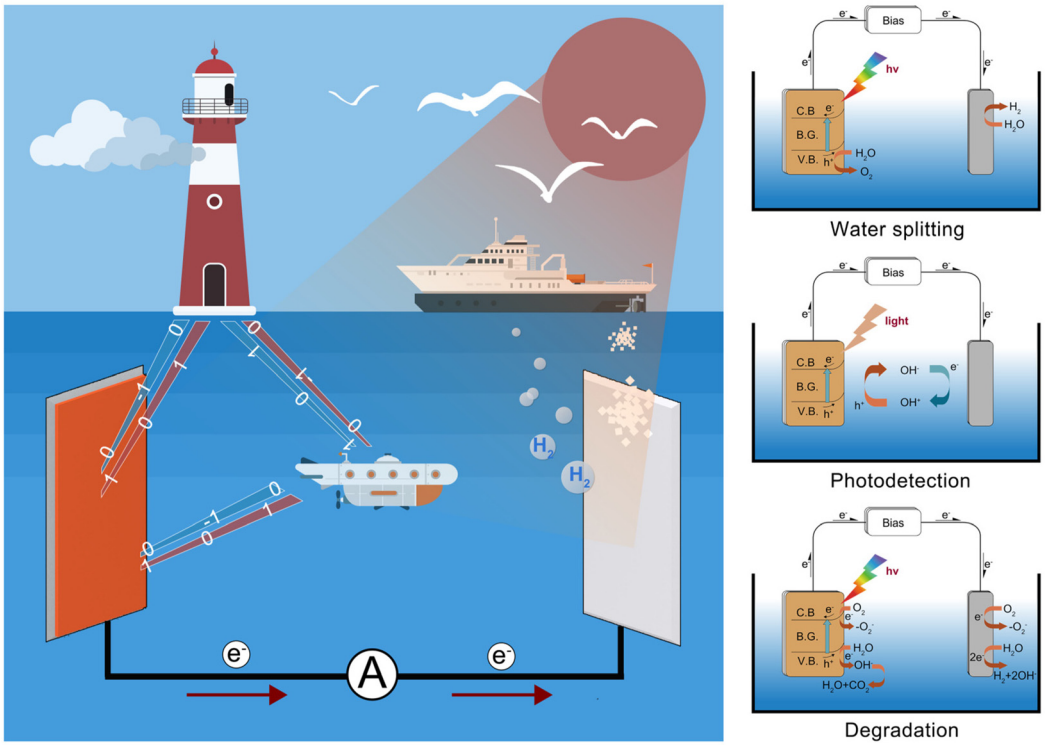

Fig. 1 Schematical mechanism for PEC activity.

element".[18] Owing to the existence of $6s^2$ lone pair electrons, bismuth ions tend to form asymmetrical coordinations with anisotropic crystal structures.[19] Hence, Bi-based ionic crystals can be used as multiferroics, superconductors, high ionic conductors, photocatalysts, and photovoltaics.[16,17,20–23]

Bismuth-based semiconductors are a class of materials with special electronic and optical structures.[13–15,20,24] Due to the positive valence band position and strong oxidation ability of most bismuth-based semiconductors, they are ideal catalysts for water splitting and photocatalytic degradation of pollutants.[25,26] The optical and electrical properties, like bandgap and carrier mobility, of bismuth-based compounds can be tuned by controlling the anion composition.[25,26] Based on these characteristics, the bandgap of bismuth-based compounds can be tuned between 0.1 eV and around 6.0 eV, suitable for broadband photoenergy conversion and detection.[25,26] Some bismuth-based compounds possessed very high carrier mobility; for example, the carrier mobility of Bi_2O_2Se reached up to 450 $cm^2 V^{-1} s^{-1}$ at room temperature, which was even higher than that of the well-investigated 2D material.[27] In addition, bismuth-based semiconductor materials have excellent chemical stability so that BiOI is stable in the laboratory environment for at least 197 days.[28] Also, very recently, the 2D in nature bismuth-based semiconductors, like BiOI and Bi_2O_2Se, have been determined as a kind of novel room-temperature ferroelectric material,[29,30] which would be fruitful for PEC-type and electrical applications.

According to the elemental composition, bismuth-based compounds can be mainly divided into binary compounds and ternary compounds. The binary compounds mainly include bismuth oxide, bismuth sulfide, bismuth selenide, bismuth telluride, *etc.*,[26,31–34] while the ternary compounds include bismuth vanadate, bismuth oxyhalides and bismuth oxychalogenides,[25,26] *etc.* Until now, there have been over 20 000 articles containing the keywords Bismuth-based compounds and PEC. Among the investigated bismuth-based semiconductors is bismuth vanadate ($BiVO_4$): $BiVO_4$ is a well-studied bismuth-based oxide that has shown promising performance as a photoanode for PEC water splitting.[35–37] $BiVO_4$ has a suitable bandgap for visible light absorption, good charge separation properties, and relatively high catalytic activity. Until now, there are a large number of review articles on $BiVO_4$.[38,39] Thus, we just summarized the progress of bismuth binary and mixed-anion compounds in this manuscript. This article mainly discussed bismuth oxide, bismuth sulfide, bismuth oxyhalides, and bismuth oxychalogenides (Fig. 2). This review first introduced the crystal structures and intrinsic properties of these compounds. Then, this article summarized the reported synthesis techniques and challenges that are faced, especially for thin films, although there are few reviews focusing on the film deposition. Lately, the recent PEC-type photodetection and water splitting was introduced and the main issue of PEC stability was analyzed. Finally, this perspective provides an outlook on the application prospects of bismuth-based semiconductors in the field of marine engineering.

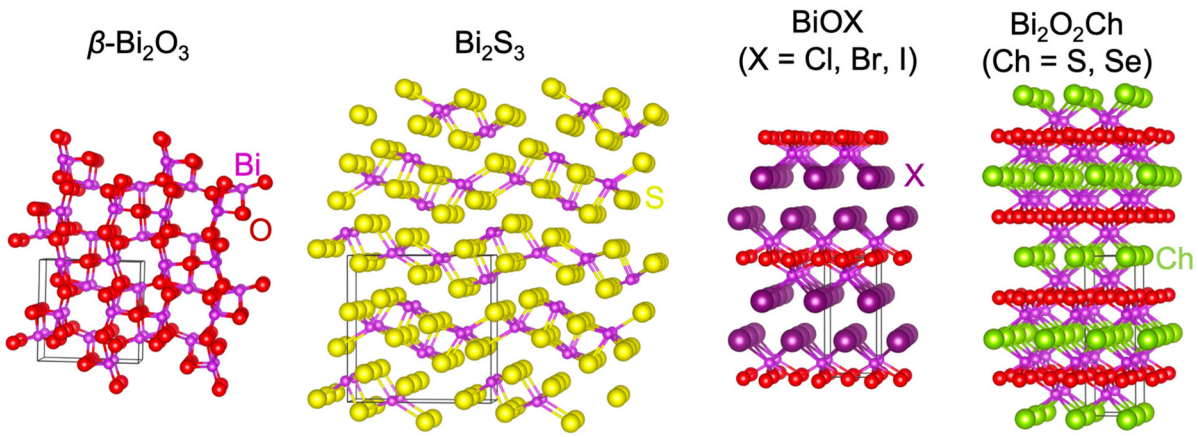

Fig. 2 Crystal structure of β-Bi_2O_3, Bi_2S_3, BiOX, and Bi_2O_2Ch.

2. Introduction of bismuth binary and mixed-anion compounds

2.1 Bismuth binary compounds

Bismuth-based binary compounds mainly include Bi_2O_3, Bi_2S_3, Bi_2Se_3, and Bi_2Te_3 *etc.*[26,31–34] Among them, Bi_2O_3 and Bi_2S_3 possessed promising photoelectric and photocatalytic properties, which were widely used in photovoltaic devices, optoelectronic devices, and photocatalytic applications.[33,34,40] Bi_2Se_3 is a kind of topological insulator with non-trivial surface states and electronic structures, demonstrating research significance in the fields of topological insulators and quantum bits.[31,41] Bi_2Te_3 is a kind of excellent thermoelectric material, which can be used as thermoelectric modules, converting waste heat into electrical energy, and demonstrates potential applications in energy utilization and energy conservation.[42,43] These bismuth binary compounds not only possess rich physical and chemical properties, but also exhibit diverse application prospects, which have important research and application significance. Due to the limitations of the topic selection, this article focused on introducing Bi_2O_3 and Bi_2S_3 for PEC-type applications.

2.1.1 Bi_2O_3. Bi_2O_3 (Fig. 3) is the simplest oxide among the bismuth-based compound families.[40] At least seven phases of Bi_2O_3 have been observed: monoclinic (α), tetragonal (β), body-centered cubic (γ), face-centered cubic (δ), triclinic (ω), hexagonal (Ω) and monoclinic phases (ε). Fig. 3 showed the transformation temperatures among α-, β-, γ-, δ-, and ε-Bi_2O_3.[40] The α and δ phases are the low- and high-temperature stable phases, while the β and γ phases are metastable (Fig. 3). To synthesize the pure phase Bi_2O_3 it is necessary to carefully control the temperature and cooling process.[40]

Generally, all the Bi_2O_3 are direct bandgap semiconductors, with a bandgap between 2–3.96 eV, depending on the crystal structure.[40] At the same time, Bi_2O_3 has a high refractive index, high dielectric constant, excellent photoconductivity, and photoluminescence properties. Among the Bi_2O_3, δ-Bi_2O_3 has a complex disordered distribution of oxygen vacancies

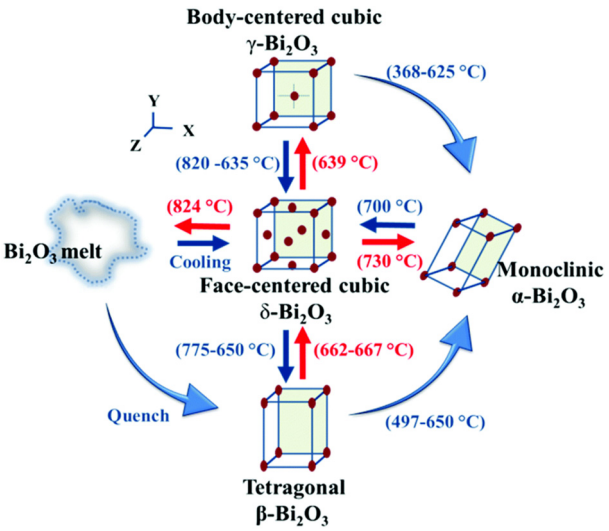

Fig. 3 Phase transformation among α-, β-, γ-, and δ-Bi_2O_3. This figure has been reproduced from ref. 40 with permission from the Royal Society of Chemistry, copyright 2021.

within the fluorite-like structure, beneficial for ionic conductivity.[44] Thus, δ-Bi_2O_3 has the highest oxygen ion conductivity and can be used as electrolyte materials for solid-state oxide fuel cells and oxygen sensors.[45]

Metastable β-Bi_2O_3 is the most attractive for photocatalysis among the Bi_2O_3, with a minimum bandgap width of 2.1–2.4 eV.[40] The narrow bandgap might be raised from the shallow valence band maximum hybridized by the Bi 6s and O 2p orbital.[46] The narrow bandgap and suitable conduction and valence band positions of β-Bi_2O_3 make it a promising photocatalyst for water splitting and other oxidation–reduction reactions.[40] In addition, β-Bi_2O_3 possessed a tunnel-like structure, where the anisotropic structure can efficiently promote the transfer of photogenerated carriers.[47] For instance, M. Kim proved the preparation of textured β-Bi_2O_3 exhibited high stability and photocurrent density owing to the short charge trans-

fer pathway.[47,48] Sometimes, α-Bi_2O_3 was used for photocatalysis, but the performance was not good owing to the large bandgap.[40] Based on these characteristics, this review mainly focuses on the β-Bi_2O_3.

2.1.2 Bi_2S_3. Bismuth sulfide (Bi_2S_3) is a binary compound that exhibits interesting optical and electrical properties.[33,34] Bi_2S_3 has been extensively researched and used in various fields, including photovoltaics, photocatalysis, sensors, and optoelectronics.[33,34] Bi_2S_3 has a rhombohedral crystal structure with the symmetry of *Pnma* and is composed of layers of bismuth atoms sandwiched between layers of sulfur atoms.[34] Seven bismuth atoms exist in two dissimilar environments, with three bismuth atoms in distant positions and four in near-plane rectangles. This layered structure contributes to its unique properties and facilitates charge transport (Fig. 2).[49]

Bi_2S_3 belongs to n-type semiconductor materials, and its conduction band is formed by hybridization of the 6p level of Bi with the 3p level of S, while the valence band is composed of the 3p level of S, and the contribution of the 6p level of Bi is the smallest.[50] The direct bandgap of bismuth sulfide is about 1.3 eV and the absorption coefficient reached about 10^4–10^5 cm^{-1}, suitable for harvesting visible light for PEC activity.[50,51] Its bandgap energy can be tuned by controlling the size, shape, and composition of the nanoparticles or thin films.[50–52] Meanwhile, Bi_2S_3 has a good electrical property. The resistivity (ρ) of Bi_2S_3 is measured at 10^5 Ω cm and the conductivity ranges from 10^{-6} to 10^{-7} Ω^{-1} cm^{-1} at 300 K.[53] The abovementioned advantages made Bi_2S_3 suitable for photocatalysts,[54,55] PEC,[56–58] photovoltaics,[59–61] energy storage,[62,63] and photothermal applications.[64]

In addition, Bi_2S_3 has attracted attention for its thermoelectric properties, which make it suitable for thermoelectric applications.[52,65,66] Thermoelectric materials can convert waste heat into usable electrical energy or provide efficient cooling by utilizing the Seebeck effect.[64,65] In this review, we just focused on the PEC-type applications and the potential applications in marine engineering.

2.2 Bismuth oxyhalide BiOX (X = Cl, Br, I)

Bismuth oxyhalide, BiOX (X = Cl, Br, I), is a class of V–VI–VII mixed-anion semiconductor materials. BiOX is a tetragonal matlockite-type layered material with the asymmetry of *P*4/*nmm*, stacking by [X–Bi–O–Bi–X] layers through van der Waals (vdW) interactions (Fig. 2). Each bismuth atom is surrounded by four oxygen and four halogen atoms in the [X–Bi–O–Bi–X] motif, producing an asymmetric decahedral symmetry. The strong intralayer covalent bonds and interlayer van der Waals attraction give BiOX anisotropic structures and properties. Due to induced polarization, this layered structure promotes the formation of an internal electrostatic field perpendicular to the layer.[67–69] The built-in electric field is considered to be beneficial for the separation of photogenerated charge carriers and enhancement of the photoelectric chemical conversion efficiency.[67–69]

For all the BiOX, the conduction band minimum is occupied by the Bi 6p orbital. The top of the valence band is dominated by the 2p orbital of the oxygen and the np orbital of the halogen.[70,71] However, the contribution of the halogen np state increases with the increase of the atomic number, resulting in a narrower band gap. Generally speaking, the band gap is BiOCl > BiOBr > BiOI in order from largest to smallest.[72] BiOI (E_g = 1.8 eV) with a smaller bandgap has better absorption performance in the visible region, while BiOCl with a larger bandgap (E_g > 3.2 eV) is better at absorbing ultraviolet light and can hardly absorb visible light.[28,72] Due to the different optical properties, these three compounds behaved differently in PEC reactions.

Carrier mobility also relied on halogen composition and crystallization orientation. Regarding the hole effective mass, BiOCl and BiOBr have a smaller mass along the [010] directions compared with BiOI.[70,73,74] Overall, BiOBr generally performs well in terms of electron mobility, followed by BiOCl and BiOI. BiOI shows a heavier electron and hole effective mass in either direction, which may be affected by its small bandgap and larger atom weight. The relatively low electron mobility of BiOCl may be limited by a large bandgap. The worse carrier mobility would lead to an increase in the recombination of the photogenerated carriers. In addition, the crystal orientation and defects may affect the electron transport performance of BiOX.[75–78] The electron effective mass of BiOX along the out-of-plane [001] direction is much smaller than the in-plane [010] direction.[70,73] Besides, several reports have indicated that the (102) preferred growth of BiOX exhibited a much superior PEC performance to that of (001) orientated BiOX, which might be attributed to the significant band bending, large carrier density, and narrower bandgap.[75,76,79] Now, the crystallographic orientation of BiOX has not been carefully controlled *via* suitable deposition techniques. In addition, there are other phases for the bismuth oxyhalides, like $Bi_4O_5X_2$, Bi_5O_7X, *etc.*, which are easily formed during the synthesis process of BiOX.[13,25,26,76] The deficiency of halogens also affected the optical and electronic structures of bismuth oxyhalides, like broadening the bandgap. Hence, further research from the point of view of experiment and theory is highly necessary. An in-depth understanding of the bandgap structure and intrinsic properties of these compounds can help guide relevant application research and materials design.

BiOX was widely investigated as the photocatalyst for pollutant degradation and water splitting for dozens of years. Recently, BiOX has been gradually used in photovoltaics like solar cells[80,81] and photodetectors,[82,83] sensors,[8,58] and piezoelectrical devices,[84,85] stimulated by their interesting physical properties. Among the BiOX, BiOBr with a moderate bandgap and carrier mobility exhibited better performance in visible light PEC reactions,[76] and BiOI showed promising performance in the construction of solar cells[80,81] and photodetection.[80,82] In summary, the selection of the appropriate material depends on the specific application requirements, which should take into account factors such as bandgap, optical properties, and electronic structure.

2.3 Bismuth oxychalogenides Bi_2O_2Ch (Ch = S, Se, Te)

Bismuth oxychalogenides, Bi_2O_2Ch, mainly include Bi_2O_2S, Bi_2O_2Se and Bi_2O_2Te.[86–88] Bi_2O_2S crystallized into orthogonal structures (Table 1 and Fig. 2), and there is a slight distortion between the adjacent $[Bi_2O_2]^{2+}$ layers.[89] The structure of Bi_2O_2Se and Bi_2O_2Te is highly symmetrical, with a tetragonal lattice (*I*4/*mmm*), where each Se^{2-} and Te^{2-} is located precisely in the center of a cube composed of 8 Bi atoms, and the $[Bi_2O_2]^{2+}$ layers are uniformly arranged along the *c*-axis. Different from the famous 2D vdWs layered materials like MoS_2, Bi_2O_2Ch is an ionic layered material in which the $[Bi_2O_2]^{2+}$ cationic layer and the $[Ch]^{2-}$ anionic layer are alternately stacked along the *c*-axis through weak electrostatic interactions. The layers are formed by strong covalent or ionic bonds within the layers, while the layers are stacked together by relatively weak electrostatic forces.[86,90] Its atomically thin layered structure allows for better electrostatic control and mechanical flexibility. Bi_2O_2X has the following advantages: (1) high carrier mobility. For example, the carrier mobility of Bi_2O_2Se reaches 450 and 40 000 $cm^2\ V^{-1}\ s^{-1}$ at 300 and 2 K, respectively, due to their small carrier effective mass.[91,92] The carrier mobility is much higher than the famous investigated 2D materials like MoS_2.[93] (2) Moderate and tunable bandgap.[86,90,94] The bandgap of Bi_2O_2Ch is highly determined by anionic elements, morphology, and thickness. The bandgap of Bi_2O_2S, Bi_2O_2Se, and Bi_2O_2Te was around 1.3, 0.8, and 0.1 eV, covering the ultraviolet to infrared band.[87,95–98] (3) Good stability at room temperature, and the bismuth element is less toxic and is abundant.[86,91,92]

The band structure characteristics of the Bi_2O_2Ch system are calculated and analyzed using first principles. The conduction band minimum of Bi_2O_2Ch is mainly composed of both the 2p orbital of the O atom and the 6p orbital of the Bi atom.[96,97] At the same time, the valence band maximum consists of the oxygen 2p orbital and the chalcogenide np orbital. As the atomic mass of the chalcogenide increases, the contribution of the oxygen 2p orbital to the electronic state decreased.[96,97] Therefore, from Bi_2O_2S to Bi_2O_2Se to Bi_2O_2Te, the bandgap decreased. The optical properties of Bi_2O_2Ch are anisotropic, as evidenced by the significant disparity in absorption intensity between the in-plane (*x*/*y*) and out-of-plane (*z*) directions, particularly within an energy range of approximately 2 eV above the absorption edge. This anisotropy aligns with the structural anisotropy of the material, where in-plane bonds exhibit strength while out-of-plane bonds are relatively weak.[99,100] The observed anisotropy and heightened absorption intensity suggest potential applications for Bi_2O_2Ch in optoelectronic devices.

Compared with bulk materials like silicon, the Bi_2O_2Ch have the advantage of flexibility, which makes them capable of overcoming short-channel effects and following Moore's law in terms of scalability.[92,101] The unique surface structure and 2D crystal structure of Bi_2O_2Se make it widely applicative in sensors, memristors and nanogenerators. Various research groups have already demonstrated the potential of Bi_2O_2Ch-based electronic devices, with Bi_2O_2Ch FETs exhibiting high carrier mobility and a large driving current.[86,94,102–104] Simple logic gates have been made from Bi_2O_2Ch. Besides, Bi_2O_2Ch is also an exceptional choice for infrared photodetectors due to its narrow bandgap and high mobility,[105–109] and its strong spin–orbit coupling effect and ferroelectricity contributing to a large thermoelectric *ZT* value.[110] Among the Bi_2O_2Ch, Bi_2O_2Se is intensively investigated followed by Bi_2O_2S. Compared with Bi_2O_2S and Bi_2O_2Se, the bandgap of Bi_2O_2Te is only about 0.1 eV, which is not suitable for application in photocatalytic hydrogen production and pollutant degradation alone.[111] Perhaps it can play a certain role as an electron transport layer and broaden the light absorption range. Given this, this review article does not discuss Bi_2O_2Te.

3. Fabrication techniques of bismuth binary and mixed-anion compounds

Generally, bismuth binary and mixed-anion compound nanoparticles have been widely synthesized through various simple techniques such as chemical precipitation, sol–gel methods, hydrothermal methods, solid phase reactions *etc.*[14,33,40] The high surface-to-volume ratio and controllable surface morphology of 3D state nanostructures have endowed various potential applications including catalysis, drug delivery, and sensors. To achieve the PEC reaction, spin-coating or drop-casting the as-synthesized nanoparticles on the conducting substrate is necessary for the photoelectrodes' construction

Table 1 Crystal structure and basic parameters of Bi_2O_2Ch. This table has been reproduced from ref. 89 with permission from Wiley, copyright 2021

Material	Crystal system	Space group	Lattice parameters (Å)	Bandgap (eV)	Effective mass (m_0)
Bi_2O_2S	Orthorhombic	*Pnnm*	a = 3.874 b = 3.84 c = 11.92	1.3 indirect	$m_e^* = 0.6$ $m_h^* = 1.04$
Bi_2O_2Se	Tetragonal	*I*4/*mmm*	a = 3.88 b = 3.88 c = 12.16	0.8 indirect	$m_e^* = 0.14$ $m_h^* = 0.86$
Bi_2O_2Te	Tetragonal	*I*4/*mmm*	a = 3.98 b = 3.98 c = 12.70	0.1 indirect	$m_e^* = 0.07$ $m_h^* = 0.76$

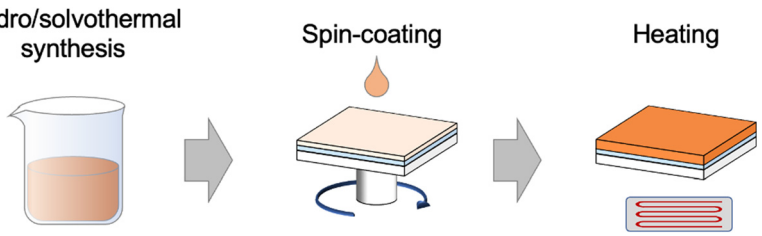

Fig. 4 Typical schematical image for the preparation of photoelectrodes from nanoparticles.

(Fig. 4). While these methods are very simple, it is challenging to fully cover the substrate with nanostructures. In addition, coated nanostructures were easily peeled off from the substrates once immersed in an electrolyte owing to the poor attachment.[14,112] Compared with the micron or nanoscale structures, continuous thin films deposited *via* advanced techniques are more suitable for the construction of large-area PEC-type devices. Besides, thin films are beneficial for the investigation of intrinsic properties such as electrical conductivity and optical coefficient. However, the deposition techniques for the thin films are usually complicated and expensive. Thus, in this part, we reviewed the fabrication techniques of bismuth binary and mixed-anion compounds from the perspective of nanoparticle synthesis and thin film deposition.

3.1 Nanoparticle synthesis

There are a large number of reports and reviews on the nanoparticle synthesis of bismuth binary and mixed-anion compounds.[14,33,40] Thus, in this part, the authors did not introduce it in detail but just point out the facing challenges and recent report.

3.1.1 Bi_2O_3. β-Bi_2O_3 nanocrystals were synthesized from bismuth nitrate and bismuth oxalate by various solution processes.[113–116] The synthesis of β-Bi_2O_3 is facing some challenges due to its specific crystal structure and properties. β-Bi_2O_3 is a metastable phase and tends to transform into the thermodynamically more stable α-Bi_2O_3 at high temperatures. Achieving pure β-Bi_2O_3 without phase transformation can be a challenge and may require specific synthesis conditions and additives to stabilize the β-phase.[40] The choice of precursor materials for the synthesis of β-Bi_2O_3 is critical. Bismuth precursors often have complex chemical behaviors, and the selection of appropriate precursors with a similar structure to β-Bi_2O_3 and reaction conditions is necessary to obtain the desired beta-phase.[117–119] In general, organometallic precursors with a similar coordination structure to β-Bi_2O_3 can be easily decomposed into β-Bi_2O_3 at the evaluated temperatures (around 400 °C).[120] Mehring 's team synthesized nanoscale-size β-Bi_2O_3 using a simple hydrolysis/annealing protocol, choosing organometallic compounds composed of $[Bi_6O_{8-x}]^{2(1+x)+}$ motifs as a precursor (Fig. 5).[120] Extending this $[Bi_6O_{8-x}]^{2(1+x)+}$ motif to an infinite network result in near-plane central cubic stacking of bismuth atoms, similar to the structure of β- and δ-Bi_2O_3.

β-Bi_2O_3 nanowires were synthesized by metal oxide vapor transport deposition and metal–organic chemical vapor deposition (CVD).[121,122] In the former method, nanoscale bismuth droplets are oxidized by O_2 at a moderate temperature of 250–350 °C, resulting in ultrathin β-Bi_2O_3 nanowires with a diameter of 7 nm and a length of several micrometers, which can be controlled by the collection zone temperature of the CVD furnace.[121,122] For metal–organic CVD, O_2 and trimethyl bismuth are used as precursors of oxygen and bismuth, respectively.[122] At 400 °C, β-Bi_2O_3 wire with a diameter between 30–90 nm is obtained, while a cluster or membrane structure is obtained between 450 °C and 500 °C. To further increase the reaction surface area, hollow microsphere-like β-Bi_2O_3 was successfully prepared by using the carbon nanospheres as sacrifice templates.[123]

In summary, choosing a suitable precursor is the prerequisite for the controllable synthesis of β-Bi_2O_3. Besides, the formation of the beta-phase is kinetically controlled. Achieving high phase purity and avoiding the conversion to the α phase often requires the precise control of reaction parameters such as temperature, reaction time, and heating/cooling rates. In addition, controlling the particle size, shape, and morphology of β-Bi_2O_3 during synthesis is still challenging. Overcoming these difficulties often requires a combination of careful experimental design, optimization of synthesis parameters, and the use of appropriate additives, precursors, or reaction conditions.

3.1.2 Bi_2S_3. Hydrothermal and solvothermal methods are the most common methods for preparing Bi_2S_3 powders in recent years, because with hydrothermal methods it is easier to achieve the morphology control of Bi_2S_3 nanostructures.[33,34] By adjusting parameters such as solution pH, temperature, pressure, reaction time, and precursor ratios, the crystallinity and morphology of the synthesized Bi_2S_3 can be tailored. So far, various morphologies of Bi_2S_3 have been prepared, including nanospheres, nanowires, nanoflowers, and nanotubes. Normally, bismuth(III) acetate, bismuth(III) citrate, $BiCl_3$, or $Bi(NO_3)_3$ was used as the Bi precursor and thioacetamide, thiourea, thiosulphate, H_2S gas, S, and Na_2S can be used as the S precursor.[33,34,124]

In the case of Bi_2S_3 synthesis, the hydrothermal approach is typically conducted at temperatures below 200 °C.[52,125,126] In some cases, continuous stirring is employed alongside the hydrothermal method. By utilizing this method, one-dimensional structures of Bi_2S_3 including nanotubes, nanowires, and

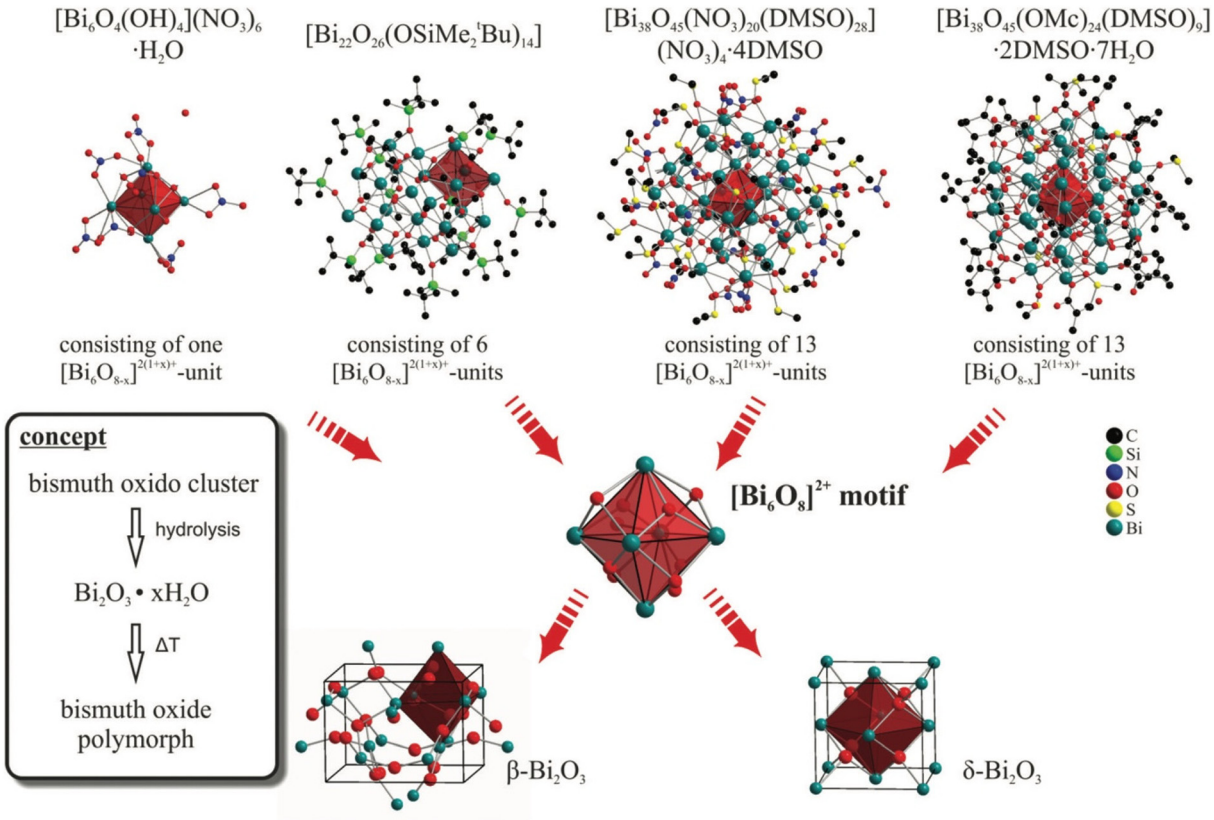

Fig. 5 Hydrolysis synthesis of β- and δ-Bi_2O_3 starting from various bismuth oxide clusters with a similar structure to Bi_2O_3.[120] This figure has been adapted/reproduced from ref. 120 with permission from the Royal Society of Chemistry, copyright 2013.

nanorods have been successfully synthesized. A unique approach involves the synthesis of hedgehog-like Bi_2S_3 micro/nanostructures using a soft-template composed of trimetallic acid and cetyltrimethylammonium bromide, which acts as a cationic surfactant.[127] Another variation of the hydrothermal method utilizes thiourea as a sulfur source, resulting in diverse Bi_2S_3 morphologies such as nanorods and nanoflowers. The reaction carried out at 180 °C involves a 2 : 3 ratio of hydrated bismuth and thiourea with the addition of nitric acid under continuous stirring.[128] Benefiting from the merits of solution-based methods, it is easy to modulate the morphology of nanoparticles by changing the solvent. To enhance the efficiency of the hydrothermal synthesis of Bi_2S_3, certain chemicals should be added, which promote the crystallization of Bi_2S_3.

Compared with hydrothermal methods, the solvothermal process requires the organic solvent as the medium for the preparation of Bi_2S_3, while the organic solvent may contain toxins and is more expensive than water. Both methods are low-cost in setup and energy. In addition, the sol–gel method,[129] mechanical milling,[130,131] microwave-assisted methods,[132] and solid phase reaction[133] were used for the synthesis of Bi_2S_3. Although these methods exhibited special merits in the synthesis of Bi_2S_3, the purity of the synthesized Bi_2S_3 is not very high owing to the difficulties in controlling the reaction process precisely. Currently, achieving the fast and green synthesis of Bi_2S_3 is highly necessary. Bismuth and sulfur precursors used in the synthesis of Bi_2S_3 can be difficult to handle due to their reactivity and sensitivity to air and moisture. Special precautions need to prevent oxidation or undesirable reactions during precursor handling and synthesis. Meanwhile, the synthesis of Bi_2S_3 involved slow reaction kinetics and required long reaction times or elevated temperatures. Optimizing the reaction conditions, such as temperature, reactant concentrations, and reaction time, is necessary to promote a complete reaction and obtain high-quality Bi_2S_3 crystals. In addition, achieving the desired stoichiometry of Bi_2S_3 can be challenging. The reaction conditions and ratios of bismuth and sulfur sources need to be carefully controlled to obtain the desired composition and avoid the formation of undesired phases or impurities.

3.1.3 BiOX (X = Cl, Br, I). Since the matlockite type of BiOX is a stable phase, various synthesis approaches have been demonstrated for the synthesis of BiOX. The most common method is a series of hydrothermal/solvothermal methods.[134–137] $Bi(NO_3)_3$ and $NaBiO_3$ were usually applied as bismuth sources, and potassium halide KX, sodium halide NaX, organic halides, and ionic liquids worked as halogen sources. BiX_3 is also used to synthesize BiOX through oxidation reactions.[134,135,138] BiOX reflected the anisotropic

crystal structure and appears in various forms depending on the synthesis method. For applications, crystals at the nanometer to micrometer scale have been studied in depth to date. This section classifies the prepared BiOX by morphology and reviews previous reports on the preparation of BiOX.

1D nanostructures like wires and fibers, owing to the large surface area–volume ratio, are suitable for photocatalytic and PEC applications. Recently, the templated method was used for the deposition of nanowires/fibers in which nano-porous anodized alumina and activated carbon fiber can be used as templates. BiOCl nanofibers were synthesized by adding polyacrylonitrile to viscous *N*,*N*-dimethylformamide solution.[139]

As for 2D sheets like BiOX, these are generally synthesized with CVD on very flat substrates, like mica and oxide single crystals.[140,141] The crystals of BiOX generally exhibit a sheet-like morphology, which is characteristic of their layered crystal structure. To synthesize these crystals, precursors such as powder BiOX and BiX_3 are placed in a reactor tube and thermally vaporized.[80,83,141] The resulting vapors are transferred onto a substrate surface positioned at a lower temperature region. By adjusting the experimental conditions and deposition time, the size of the crystals can be controlled, typically ranging from micro- to nano-scale in the lateral direction and the vertical direction, respectively.[77] These crystals often possess a flat surface, making them suitable for constructing multilayer devices and facilitating the measurement of physical properties such as conductivity.

Compared with 1D and 2D BiOX, 3D BiOX, like nanoflowers, was easily formed during the synthesis process. These 3D nanostructures are typically composed of aggregated 2D sheets, reflecting the layered crystal structure and its anisotropic nature.[142–144] The morphology of these microcrystals is heavily influenced by experimental conditions, including the pH and reaction temperature. For instance, a solution containing $Bi(NO_3)_3$ dissolved in nitric acid can be subjected to heat treatment with the addition of sodium halide, polyvinylpyrrolidone, and citric acid to produce spherical microstructures of BiOX.[145,146] The halogen composition can be precisely controlled by adjusting the concentration of sodium halide, which is a significant advantage of the solution-based process. The concentration of additives, such as polyvinylpyrrolidone and citric acid, plays a crucial role in determining the morphology of the resulting microstructures.[145,146] In the solvothermal reaction, where $BiCl_3$ is dissolved in a mixture of ethanol and water, the morphology of BiOCl can be altered by varying the concentration of citric acid.[145] Nanosheets can transform into nanoplates, and nested structures can form hollow spheres as the concentration of citric acid is increased. This result demonstrates that citric acid not only serves as a crystal growth inducer but also acts as a structural guide agent, influencing the morphology of BiOCl.

Recently, solvent-free mechanical grinding methods have also been used for the preparation of BiOX (Fig. 6).[135] BiOX fractional flower-like nanostructures were synthesized by mixing and grinding $Bi(NO_3)_3$ with KX. During the grinding, the HNO_3 acid formed in the product promotes the further reaction of $Bi(NO_3)_3$ and the nucleation of BiOX. With the increase in grinding time, the single-layer laminate was assembled into a flower-like nanostructure. This method is much simpler and greener than the conventional solvent-based synthesis techniques, which are suitable for industrial application. However, further optimization of the synthesis condition is necessary to enhance the purity and control the surface morphology of BiOX. Besides, achieving and maintaining the desired stoichiometry of bismuth oxyhalide nanoparticles is challenging. Variations in the reaction parameters, such as temperature, time, precursor concentration, and other reaction conditions, can impact the stoichiometry and composition of the synthesized nanoparticles. In addition, BiOX nanoparticles are prone to aggregation or stability issues, leading to unwanted particle growth or changes in properties. Incorporating appropriate stabilizing agents or surface modifications, such as surfactants or ligands, can enhance the stability and prevent the aggregation of the nanoparticles.

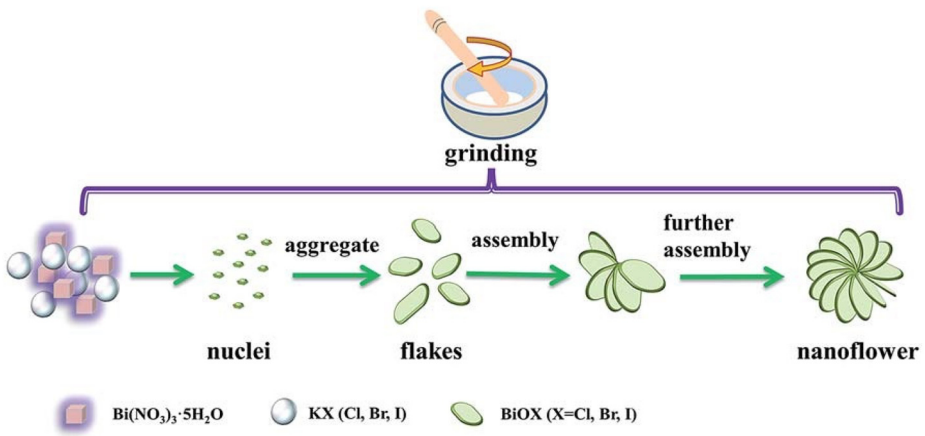

Fig. 6 Solvent-free synthesis process scheme of BiOX through grinding methods.[135] This figure has been adapted/reproduced from ref. 135 with permission from the Royal Society of Chemistry, copyright 2018.

3.1.4 Bi_2O_2Ch (Ch = S, Se). The hydrothermal method is the main method for the synthesis of Bi_2O_2Ch nanopowders. $Bi(NO_3)_3{\cdot}5H_2O$ and $SC(NH_2)_2$ have been widely used as precursors in alkaline environments for the synthesis of Bi_2O_2S.[147–150] $Bi(NO_3)_3$ is hydrolyzed in an alkaline solution to produce $BiONO_3$, and the generated $BiONO_3$ reacts with $SC(NH_2)_2$ to produce Bi_2O_2S. Similarly, Ghosh *et al.* obtained two-dimensional Bi_2O_2Se sheets at room temperature by reacting $(SeC(NH_2)_2)$ and $Bi(NO_3)_3$ in alkaline solutions.[30,151–154] The alkaline solution is probably conducive to the hydrolysis of $Bi(NO_3)_3$ to $BiONO_3$ and the decomposition of $SeC(NH_2)_2$ to Se^{2-}. Subsequently, $BiONO_3$ reacted with Se^{2-}, forming Bi_2O_2Se nanosheets. Sometimes, reductants like $NaBH_4$ were used for the reduction of Se.[151,154] Although the hydrothermal method possessed various advantages, the size and thickness control of two-dimensional Bi_2O_2X is still not ideal, which is appropriately attenuated by controlling the specific growth direction of the precursor. However, it should be carefully avoiding the oxidation of Se ions owing to its poor stability, especially in air. The detailed chemical reaction mechanism for the synthesis of Bi_2O_2Ch was still in dispute. Clarifying the mechanism would be beneficial for the synthesis of high-quality Bi_2O_2Ch. In addition, grounding the S and bismuth oxide aided by NaOH induced a disproportionation reaction of sulfur, promoting the preparation of Bi_2O_2S.[155] The ball milling method is very simple, while it is hard to remove impurities like S. Compared with other bismuth binary and ternary compounds, Bi_2O_2Ch is still at the very early stage and the synthesis technique is not very mature. One possible reason is the difficulties in choosing suitable precursors. To further the Bi_2O_2Ch practical applications, finding alternatives to the expensive $SeC(NH_2)_2$ is highly necessary.

3.2 Thin film deposition

Although thin film is much more suitable for the PEC-type applications, the number of reports on the thin film deposition of bismuth binary and mixed-anion compounds is much less than that on the format of nanopowders. Also, compared with well-investigated oxide and 2D materials, the deposition techniques of bismuth binary and mixed-anion compounds still need further investigation. This part mainly discussed the previously reported film deposition techniques for the bismuth binary and mixed-anion compounds and pointed out the challenges.

3.2.1 Bi_2O_3. As mentioned in section 2, general heat treatment to synthesize β-Bi_2O_3 tends to form a stable α-Bi_2O_3 or polyphase owing to the thermal stability of Bi_2O_3. However, some combinations of appropriate methods, precursors, and conditions can stabilize β-Bi_2O_3. Table 2 summarized the reported deposition techniques for β-Bi_2O_3 thin films. Synthesis methods for β-Bi_2O_3 can be divided into: (1) physical vapor deposition, (2) chemical vapor deposition, and (3) solution-based film deposition methods. For physical vapor deposition methods such as thermal evaporation and sputtering, precursors like Bi and Bi_2O_3 are evaporated into atoms and/or ions by applying high energy in a high vacuum environment.[156–159] These species are then deposited onto heated substrates. However, the high temperatures that are typically required for crystallizing the oxide can be challenging when dealing with volatile bismuth. Moreover, in a vacuum environment at high temperatures, Bi^{3+} ions are readily reduced to elemental Bi (0).[160] Hence, previous studies have utilized these techniques to deposit metallic bismuth films and/or amorphous BiO_x precursor films at low temperatures. Subsequently, these films were crystallized to β-Bi_2O_3 through annealing in air. For instance, nanoporous films were synthesized from metallic bismuth films on fluorine-doped tin oxide glass substrates, while (201) oriented films were prepared using a Bi/BiO_x double-layer approach on glass substrates.[156,157]

CVD involves transferring gaseous precursors onto a heated substrate surface, where they undergo a chemical reaction to form a thin film.[162] The quality of the film largely depends on the specific precursor used. In previous studies on the chemical vapor deposition of β-Bi_2O_3, bismuth(III) *tert*-butanol was used as a precursor, resulting in microcrystals with diameters ranging from 0.4 to 2 μm.[162] By controlling the flow rate of bismuth precursors, homogeneous β-Bi_2O_3 films were successfully obtained on Si (100) and Al_2O_3 substrates.[170]

Table 2 Previous synthetic approaches for β-Bi_2O_3

Method		Temperature	Precursor	Ref.
PVD	Thermal evaporation and post annealing	Annealing at 300 °C	Bi (001) film, BiO_x amorphous film	156
	Sputtering and post annealing	200–600 °C	Bismuth metal, Bi_2O_3	157–159
CVD	Aerosol-assisted CVD	300–450 °C	Bismuth carbamate	161
	MOCVD	450 °C	$Bi(OtBu)_3$	162
	Mist CVD	350–600 °C	Bismuth(III) 2-ethylhexanoate	163
Solution-based techniques	Photochemical synthesis	250 °C	Bismuth(III)-*N*-methyldiethanolamine complex	45
	Spray pyrolysis	450 °C	Bismuth(III) acetate	164
	Spin-coating and post annealing	370 °C	$Bi_{38}O_{45}(OMc)_{24}(DMSO)_9{\cdot}2DMSO{\cdot}7H_2O$	165
		300–450 °C	$Bi(NO_3)_3{\cdot}5H_2O$	166
	Electrodeposition and post annealing	RT and annealing at 200–600 °C	$Bi(NO_3)_3{\cdot}5H_2O$, acid/NaOH	167 and 168
	Microwave-assisted chemical synthesis and post annealing	300 °C	$Bi(NO_3)_3{\cdot}5H_2O$	169

In comparison with traditional physical and chemical vapor deposition methods, the solution deposition method is commonly employed for the thin film growth of β-Bi_2O_3.[45,164–169,171] This approach offers several advantages, such as the wide choice of precursors and a simple experimental setup that can be adjusted based on the chemical properties of the reactants and products. Atmospheric pressure is favorable for preventing bismuth evaporation, while low temperatures are conducive to obtaining metastable β-Bi_2O_3. Various solution-based methods for β-Bi_2O_3 deposition have been reported. For example, one approach involves the ultrasonic spraying of a tetrahydrofuran solution containing $[Bi_{38}O_{45}(O_2CC_3H_5)_{24}(DMSO)_9]\cdot 2DMSO\cdot 7H_2O$, which is then hydrolyzed and annealed to obtain a thin film with an α- or β-Bi_2O_3 bulk structure at 550 and 370 °C, respectively.[165]

In another report, a solution of bismuth(III) *N*-methyldiethanolamine was spun onto a glass or polyimide substrate to form an amorphous film that crystallized to β-Bi_2O_3 under ultraviolet irradiation in O_2 at 250 °C (Fig. 7a).[45] Deposition from bismuth metal electrodes at room temperature by electrochemical methods has been reported (Fig. 7b).[167,168,171] β-Bi_2O_3 films are formed on platinum or graphite rods by the anodic oxidation of citric acid or NaOH aqueous solutions, and subsequent annealing improves the crystallinity of the films. To achieve the electrochemical deposition, the substrate is limited to conducting materials. Very recently, (201) β-Bi_2O_3 epitaxial thin films on α-Al_2O_3 (0001) single crystal substrates were deposited through mist CVD *via* choosing bismuth(III) 2-ethylhexanoate as the precursor (Fig. 7c). The morphology and crystallinity of β-Bi_2O_3 were highly dependent on the deposition temperature: a high temperature led to the aggregation of thin films and a low temperature resulted in formation of the amorphous film. Short-time high-temperature (600 °C) post-annealing was beneficial for the enhancement of the crystallinity and surface flatness, while slightly long-time annealing will cause the degradation of thin film quality (surface roughness and crystallinity).[163] As far as we know, this is the first report on the epitaxial growth of β-Bi_2O_3; however, owing to the complicated deposition process, this method is not suitable for industrial application.

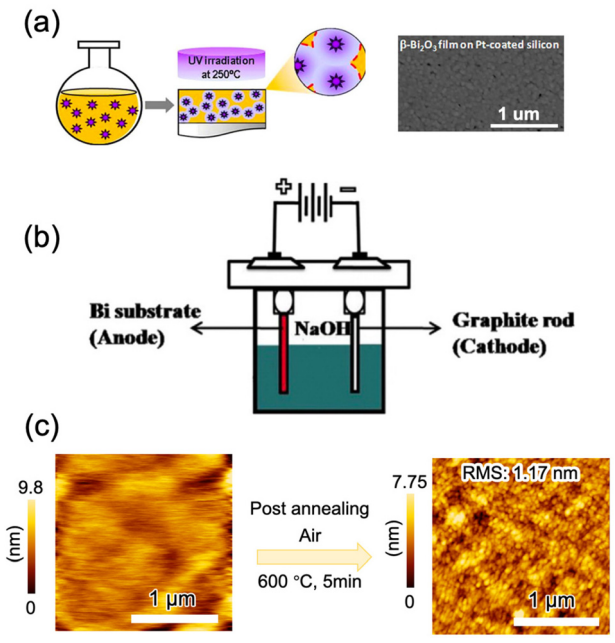

Fig. 7 β-Bi_2O_3 thin film deposited by (a) a photochemical solution method,[45] adapted from ref. 45 with permission from Springer Nature, copyright 2016; (b) electrochemical deposition,[172] adapted from ref. 172 with permission from Elsevier, copyright 2016; and (c) solid-phase epitaxy *via* mist CVD,[163] adapted from ref. 163 with permission from the American Chemical Society, copyright, copyright 2019.

Similar to nanoparticles, special synthesis techniques, optimization of deposition conditions, and the inclusion of additives may be necessary to stabilize the β phase and prevent phase transformation. Normally, post annealing to improve the crystallinity of β-Bi_2O_3 is necessary for most film deposition methods, which posed challenges in controlling phase purity and energy saving. In addition, annealing at higher temperatures than 200 °C would cause the decomposition of β-Bi_2O_3. In that sense, annealing at high temperatures to stabilize β-Bi_2O_3 is not a good method. Meanwhile, organic compounds are usually used as precursors for the deposition of β-Bi_2O_3, where the issue of carbon residues needs to be considered. To some extent, carbon residues will degrade the photoresponse performance. Thus, overcoming these challenges is necessary for the broad practical usage of β-Bi_2O_3.

3.2.2 Bi_2S_3. Bi_2S_3 thin films have been obtained through various deposition techniques such as CVD, chemical bath deposition (CBD), spin-coating, and spray pyrolysis,[50,59,173–177] as listed in Table 3. Spin-coating is one of the simplest film deposition methods. Bismuth acetate and propionic acid were used as precursors to form amorphous Bi_2S_3 films and then annealed them in H_2S gas to achieve the crystallization process (Fig. 8a).[176] The as-prepared Bi_2S_3 films possessed a relatively small surface roughness and large grain size. The successive ionic layer absorption reaction (SILAR) method is also known as an improvement for chemical bath deposition. Bismuth acetate was used as a cationic precursor to provide Bi^{3+}, and thioacetamide as an anionic precursor to provide S^{2-}. The thickness of the Bi_2S_3 films can be controlled *via* the deposition cycles. CVD has been used for the deposition of Bi_2S_3 *via* sulfidation of the Bi_2O_3 thin films with a two-step synthesis method (Fig. 8b).[178] However, post-annealing is needed for most thin film deposition strategies as shown in Table 3. It should be noted that too short and too long an annealing time result in partial crystallization and the formation of impurities, respectively.[50,176] Besides, there are still other various drawbacks for the Bi_2S_3 film deposition techniques, like the requirement for toxic and expensive precursors, difficulty in controlling the surface morphology, a long reaction time, *etc.*[178,179] Among the reported techniques, MOCVD has the flexibility of choosing suitable precursors to achieve the efficient synthesis of Bi_2S_3 so that the deposition process is simple and time-saving. However, the synthesis

Table 3 Previous synthetic approaches for Bi_2S_3

Technique		Precursors	Process	Ref.
Two-step	Electrochemical deposition	CH_3CSNH_2, $C_{12}H_{10}BiK_3O_{14}$ or $Bi(NO_3)_3{\cdot}5H_2O$	(1) Deposition of bismuth film (2) Oxidized into Bi_2O_3 (3) Vulcanized to Bi_2S_3	182 and 183
	Sputtering and solution-assisted method	Bi_2O_3, CH_4N_2S	(1) Synthesis of Bi_2O_3 thin film by radiofrequency sputtering (2) Hydrothermal treatment for 3 h	179
	Chemical vapor deposition (CVD)	Bi metal, S	(1) Synthesis of Bi_2O_3 exfoliated from Bi (2) Vulcanized to Bi_2S_3	178
	Spin coating	$Bi(NO_3)_3{\cdot}5H_2O$, $Na_2S{\cdot}9H_2O$	(1) Synthesis of Bi_2S_3 powder (2) Film deposition	184
		$C_6H_9BiO_6$, CH_4N_2S	(1) Deposition of amorphous Bi_2S_3 film (2) Crystallized under H_2S gas	176
	Hydrothermal method	$Na_2S_2O_3$, $Bi(NO_3)_3$	(1) Deposition of intermediates films at 600 °C for 12 h (2) Annealed at 150–250 °C	185
	Successive ionic layer adsorption and reaction	$Bi(NO_3)_3$, $Na_2S{\cdot}9H_2O$	(1) Two-step dipping process (2) Post annealing	186
One-step	CVD	Bi_2S_3 nanopowders	Evaporation of precursor at 600 °C and deposited at 500 °C	59
	Metal–organic CVD	Secondary amine, CS_2, Bi_2O_3	(1) Synthesis of the metal–organic precursor $Bi(S_2CNEt_2)_3$ (2) Film deposition	180
	Mist CVD	$BiCl_3$, thiourea	Dissolved in DMF solvent, atomized into mist, deposited at 450 °C	181

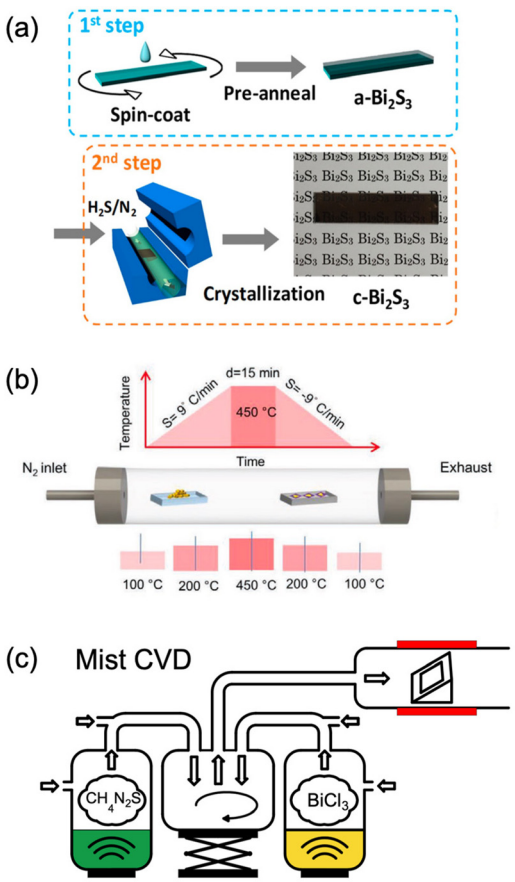

Fig. 8 Bi_2S_3 deposited by (a) spin-coating method,[176] adapted from ref. 176 with permission from the American Chemical Society, copyright 2018; (b) CVD deposition,[178] adapted from ref. 178 with permission from Wiley, copyright 2020; and (c) dual-source mist CVD,[181] adapted from ref. 181 with permission from the American Chemical Society, copyright 2022.

process of metal–organic compounds $Bi(S_2CNEt_2)_3$ is too complicated and this compound is toxic.[180]

Very recently, mist CVD, a kind of green and open-air pressure solution-based method, has demonstrated the fast deposition of Bi_2S_3 thin films *via* applying the less toxic, cheap, and commercially available $BiCl_3$ and thiourea as the precursors (Fig. 8c).[181] To our knowledge, this is the simplest method for the synthesis of high-quality Bi_2S_3 film, while the surface morphology is rough and discontinuous. Hence, developing facile techniques to prepare uniform and continuous Bi_2S_3 thin films is still highly necessary. Until now, discontinuous thin films were obtained in which the synthesized Bi_2S_3 thin films were composed of nanowires and/or nanoplates. Especially, enormous efforts should be devoted to the surface morphology modulation of Bi_2S_3 thin films.[181] Besides, the crystallization temperature is normally higher than 400 °C which is not suitable for some organic-based flexible substrates and energy saving. Besides, there are no epitaxial Bi_2S_3 thin films, which might be attributed to the anisotropic crystal structure. Thus, finding suitable precursors to decrease the deposition temperature of Bi_2S_3 may be beneficial for broadening the application of Bi_2S_3.

3.3 BiOX (X = Cl, Br, I)

CVD is one of the most commonly used techniques for the deposition of BiOX from bismuth halides. Dating back to 1998, BiO_xI_y thin films were deposited on MgO (100) substrates with CVD from BiI_3 and O_2.[187] In the conditions examined, the growth window of stoichiometric BiOI was very small, and iodine deficiency was observed in the most of checking experimental conditions. In addition, the surface of the substrate was not fully covered by the film. Recently, BiOX in the format

of nanoplates with the size of around tens of micrometers was deposited *via* CVD in which the substrate is not fully covered by the nanoplates (Fig. 9a).[80,82,83,141,188–191] Currently, there are nearly no reports of BiOX thin films deposited *via* the vacuum-based technique, which might be attributed to the difficulty of controlling the chemical composition due to very volatile halides and bismuth.

Instead, solution-based approaches for depositing continuous BiOX thin films are frequently documented.[76,79,192–196] One of the simplest methods is the SILAR method (Fig. 9b).[193] Immersing the glass substrate coated with FTO in a solution containing bismuth and halogen precursors resulted in the formation of a BiOX film.[193] The film comprises aggregated nanosheets that grow vertically on the substrate. Immersing the substrate in HF, HCl, and KBr solution also facilitates the conversion of Bi_2O_3 film into BiOX at room temperature.[72] However, the conversion is not fully complete for bismuth oxyiodide. As in the case of the SILAR method, the obtained film consists of nanosheets.

Another straightforward solution-based technique is spray pyrolysis.[197] In this process, a solution of $Bi(NO_3)_3$ and NH_4I glycol solutions is sprayed onto a heated substrate, where a film is formed through the evaporation and chemical reaction of the precursor. The deposition temperature played a crucial role in determining the morphology and composition of the films.[197] Like the impregnation method, the resulting film is composed of nanosheets. AACVD, combing the merits of vapor and solution deposition techniques, is applied to BiOX films (Fig. 9c).[76,194] The bismuth halide *N*,*N*-dimethylformamide solution was atomized with a piezoelectric device and transferred to a heated FTO-coated glass substrate. The resulting film consists of nanosheets with improved flatness and density. Very recently, mist CVD, similar to AACVD, was widely used for the deposition of BiOX epitaxial and polycrystalline thin films. By choosing perovskite-type oxides like $SrTiO_3$ as the substrates, the BiOX showed epitaxial growth so that the obtained thin film possessed high crystallinity and an atomic flat surface.[198] Also, on the polycrystalline conducting glass substrate, the preferred orientation of BiOX was tuned by controlling the deposition temperatures.[79,195,196] Also, the thickness of BiOX thin films was controlled by tuning the precursor concentration and deposition time.[189,198] However, it is very hard to obtain very thick BiOX thin films with mist CVD. In addition, BiX_3 is very easily hydrolysed into other compounds which is not suitable for the deposition of BiOX. Adding an acid reagent can prevent the hydrolysis of BiX_3, which also degrades the obtained BiOX thin films. The epitaxial thin films are suitable for the construction of high-performance PEC-type devices. However, the epitaxial growth is highly dependent on the single crystal substrates. Until now, commercially available conducting single crystal substrates have been very limited. Overall, finding suitable precursors, substrates, and deposition techniques is highly necessary for the deposition of BiOX thin films.

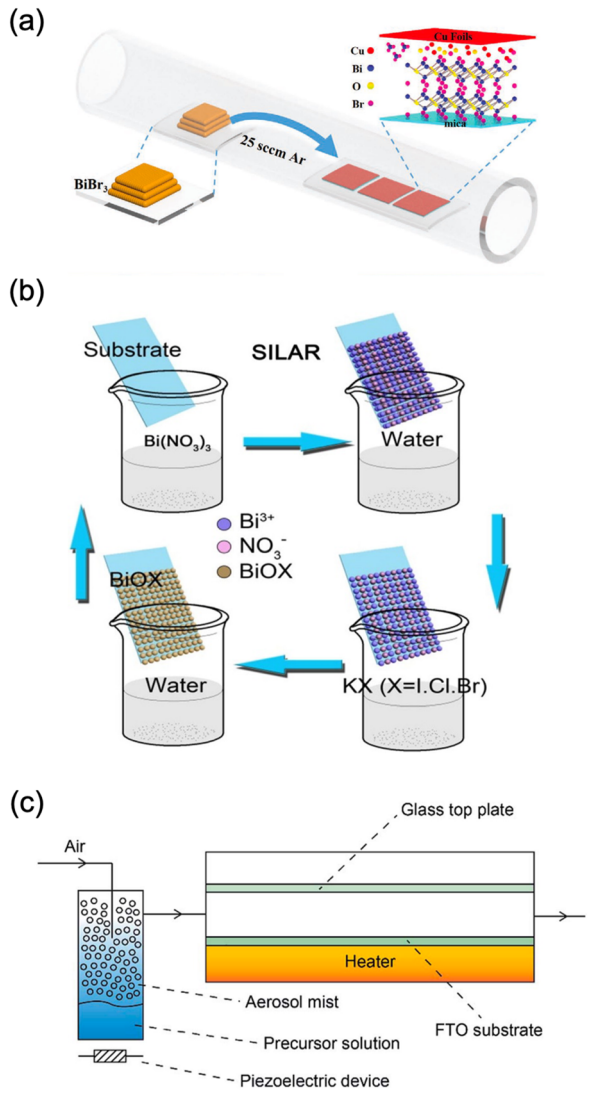

Fig. 9 Schematic diagram of preparing BiOX thin films using (c) CVD,[83] adapted from ref. 83 with permission from Wiley, copyright 2020; (b) SILAR,[193] adapted from ref. 193 with permission from Wiley, Elsevier, copyright 2018; and (c) aerosol-assisted CVD.[76] adapted from ref. 76 with permission from the Royal Society of Chemistry, copyright 2016.

3.4 Bi_2O_2Ch (X = S, Se)

Attracted by the very high carrier mobility of Bi_2O_2Ch, film deposition techniques have shown great improvement during recent years. At present, the Bi_2O_2Ch film deposition techniques mainly include the liquid phase method,[101,199] physical/chemical vapor deposition,[200] molecular beam epitaxy,[201] and other technologies.[150,199] Table 4 briefly summarized the reported Bi_2O_2Ch thin film deposition techniques. Bi_2O_2S films are mainly prepared by chemical bath deposition and spin coating. $Bi(NO_3)_3{\cdot}5H_2O$ and thiourea or Na_2S were used as precursors, and alkaline solutions (KOH, NaOH) were added to accelerate the formation of Bi_2O_2S. The reaction time of the Bi_2O_2S prepared by this method is usually long, and the surface of the Bi_2O_2S prepared is rough and nanoflower-like.[147,150,202] The primary method for preparing Bi_2O_2Se is

Table 4 Previous synthetic approaches for Bi_2O_2Ch thin films

	Method	Bi Source	Ch Source	Condition	Sample form	Ref.
Bi_2O_2S	Hydrothermal + spin coating	$Bi(NO_3)_3{\cdot}5H_2O$	Thiourea	Alkaline solution, 12 h	Nanosheet ~ 100 nm	147
		$C_6H_{13}BiN_2O_7{\cdot}H_2O$	Thiourea	KOH solution	Nanosheet ~ 2 μm	150
		Bi_2O_3	Thiourea	40 h, 180 °C	Nanosheet ~ 100 nm	202
	Chemical bath deposition	$Bi(NO_3)_3{\cdot}5H_2O$	Thiourea	200 °C, 80 min	Nano-flower-like film	199
		$Bi(NO_3)_3{\cdot}5H_2O$	Na_2S	30 °C, 4 h	Continuous film	205
Bi_2O_2Se	CVD	Bi_2O_3, Bi_2Se_3		500–700 °C	Nanosheet ~ 200 μm	140
		Bi_2O_3	Se	680 °C	Nanosheet ~ 250 μm	91
		Bi_2Se_3, O_2		Salt assisted, 500 °C	Nanosheet ~ 500 μm	203
	MOCVD	$Bi(Ph)_3$, $(CH_3)_2Se_2$		350 °C	Epitaxial thin films	204
	Pulsed laser deposition	Bi_2O_2Se prepared by Bi_2O_3, Bi, Se		375 °C, $0.71Pb(Mg_{1/3}Nb_{2/3})O_3$–$0.29PbTiO_3$	Epitaxial thin films	200
	Molecular beam epitaxy	Bi	Se	$SrTiO_3$	Epitaxial thin films	201
	Hydrothermal + spin coating	$Bi(NH_3)_2C_6H_7O_7$	Na_2SeO_3	Alkaline solution, 12 h	Nanosheet ~ 2 μm	150
	Solution-assisted	Bi_2O_3 film by spin coating	Se	Air annealed, selenized	Continuous film	101

chemical vapor deposition, which typically uses Bi_2O_3 or Bi_2Se_3 as the precursor.[91,140,203] By precisely controlling the parameters of the film deposition and selenization or oxidation processes, the deposition of Bi_2O_2Se films can be successfully achieved (Fig. 10a). Bi_2O_2Se epitaxial thin films with precise control over thickness down to the monolayer were demonstrated on TiO_2-terminated $SrTiO_3$ through MOCVD.[204] In addition, high-quality Bi_2O_2Se epitaxial thin films with high crystallinity and a flat surface have been synthesized by molecular beam epitaxy (MBE, Fig. 10b).[201] However, the MBE method is not suitable for industrial-scale production owing to the expensive setup and difficulties in the synthesis of large-size epitaxial thin films.[201]

In recent studies, wafer-scale Bi_2O_2Se epitaxial thin films have been successfully grown on perovskite-type oxide single crystal substrates such as $LaAlO_3$, $SrTiO_3$, and (La, Sr)(Al, Ta)O_3.[86,204,206] These perovskite-type oxides possess a similar crystal structure to Bi_2O_2Se, resulting in a small lattice mismatch between the substrate and the film. By utilizing these perovskite-type oxide single crystals as substrates, high-quality Bi_2O_2Se thin films with controllable thicknesses and wafer sizes were obtained.[206] Except for the small lattice mismatch, the strong interatomic interaction at the interface of the Bi_2O_2Se and $SrTiO_3$ promoted the epitaxial growth of Bi_2O_2Se, which initiates at the Bi–O layer at the $SrTiO_3$ interface.[204] These findings emphasized the significance of selecting suitable substrates for achieving large-size 2D single crystals and provided insights for the synthesis of large-size Bi_2O_2S and Bi_2O_2Se epitaxial thin films.

To achieve the epitaxial growth of Bi_2O_2Se, it is commonly necessary to utilize oxide single-crystal substrates. However, there are several challenges arising from the limitations associated with these substrates. The size of the oxide single crystal substrate limits the preparation of large-size Bi_2O_2Se epitaxial thin films.[86,206,207] Most of these substrates are insulators, which are not suitable for the construction of PEC-type devices. Achieving the exfoliation of thin film is necessary. However, the Bi_2O_2Se epitaxial thin films grown on oxide single crystal substrates are limited by the strong binding force between the Bi_2O_2Se and the substrate, making it difficult to exfoliate the thin film from the substrate.[208,209] Additionally, Bi_2O_2Se grown on a mica substrate is prone to achieving thin film exfoliation and transfer, but mica is hard to remove completetly during the transfer process.[208,209] Besides, some perovskite-type oxide single crystal substrates are expensive and not suitable for large-scale applications.

Although the advanced thin film techniques, like CVD and MBE,[200,201] exhibited various advantages in high-quality Bi_2O_2Se thin film deposition; these abovementioned thin film deposition methods have high requirements for atmosphere and temperature, and the deposition equipment is relatively expensive. Compared with these techniques, solution-based techniques probably achieve the facile synthesis of Bi_2O_2Se thin films.[210–212] The solution-assisted method first spin-coated Bi_2O_3 thin films, which were annealed under Se vapor to generate Bi_2O_2Se (Fig. 10c).[101] The prepared thin film has a

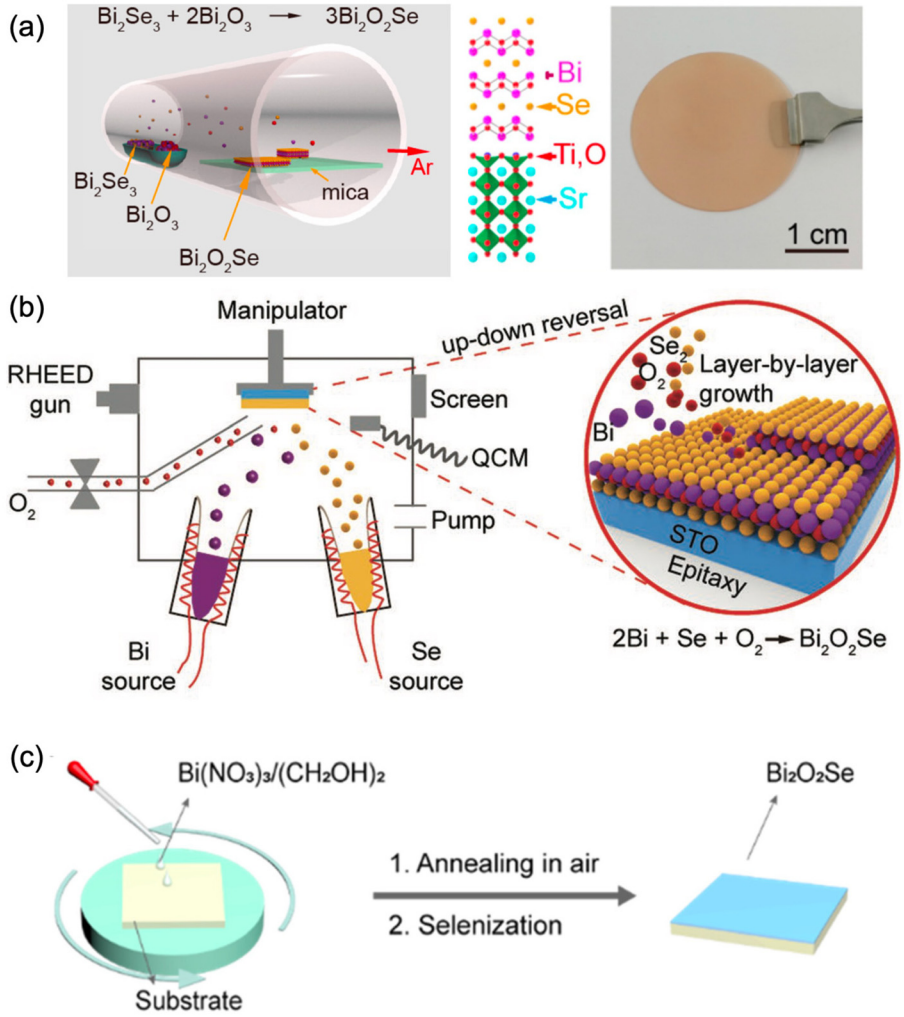

Fig. 10 Schematic diagram of preparing Bi_2O_2Se thin films using (a) CVD,[206,207] adapted from ref. 206 and 207 with permission from the American Chemical Society, copyright 2017 and 2019; (b) molecular beam epitaxy,[201] adapted from ref. 201 with permission from Wiley, copyright 2019 and (c) solution-assisted deposition with spin-coating deposition and annealing,[101] adapted from ref. 101 with permission from the American Chemical Society, copyright 2019.

large size of 2 cm, a controllable thickness, and a continuous and smooth surface, demonstrating high potential in the large-scale preparation of Bi_2O_2Se. However, there are few reports on the efficient preparation of Bi_2O_2Se thin films using solution-based deposition techniques, possibly due to the limitations of traditional liquid-phase methods in precursor selection and film rate control. To achieve the efficient preparation of Bi_2O_2Se thin films by the liquid-phase method, further optimization is needed in selecting suitable precursors, simplifying the deposition process, improving the quality of thin films, and preparing large-sized thin films.

For the deposition of Bi_2O_2Se and Bi_2O_2S, it is very important to ensure the phase purity as Bi_2Se_3 or Bi_2S_3 might be formed during the synthesis process.[213] Therefore, conditions such as temperature, pressure, and reaction time affected phase purity and crystallinity. In addition, the morphology of the material determined its application in photoelectric chemistry and photocatalysis. It may be necessary to achieve the preparation of Bi_2O_2Se and Bi_2O_2S with specific morphologies, like nanoflower or nanowire. As pointed out in the nanoparticle part, understanding the crystal growth mechanism of Bi_2O_2Se is necessary. By overcoming these challenges, high-quality Bi_2O_2Se and Bi_2O_2S thin films can be facilely synthesized, and their application potential in PEC, photocatalysis, photovoltaic, and other fields can be expanded.

4. PEC applications of bismuth binary and mixed-anion compounds

4.1 PEC-type photodetection

PEC-type photodetectors are a class of photodetectors that utilize the photoelectrochemical reaction to convert light into electrical signals. PEC-type photodetectors consist of a photoactive material, electrolyte, and appropriate electrode configurations (Fig. 11).[7,214,215] The photoactive material serves as a

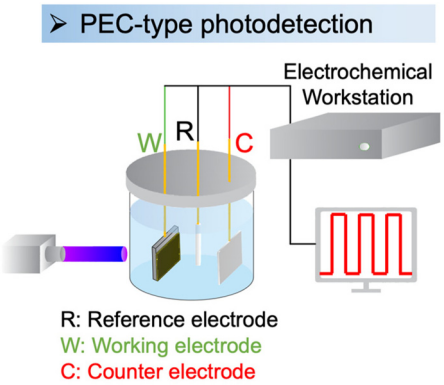

Fig. 11 Setup of a PEC-type photodetector.[216] This figure was adapted from ref. 216 with permission from Wiley, copyright 2024.

light absorber and generates electron–hole pairs when exposed to light. These photoexcited charge carriers then migrate to the electrode–electrolyte interface, where they engage in redox reactions with the electrolyte. The resulting photocurrent or photovoltage is measured to detect and quantify the incident light.

PEC-type photodetectors offer several advantages, such as high sensitivity, tunable spectral response, and the ability to operate under various lighting conditions.[7,214,215] They are highly sensitive to light due to their efficient conversion of absorbed photons into photocurrent or photovoltage. The spectral response of PEC-type photodetectors can be tuned by selecting or engineering the photoactive materials with specific bandgaps. Moreover, PEC-type photodetectors can be designed to be flexible and conformable, enabling integration onto unconventional substrates or curved surfaces. This flexibility opens up opportunities for use in wearable devices, flexible electronics, and integrated systems.

Different types of photoactive material can be utilized in PEC-type photodetectors, including semiconductor materials like metal oxides, organic semiconductors, quantum dots, or hybrid structures. The choice of materials depends on factors such as the desired spectral response, stability, and efficiency. Additionally, PEC-type photodetectors can be combined with other functionalities, such as energy conversion or sensing capabilities, to create multifunctional devices. This integration enables the development of compact and versatile systems for various applications. Overall, PEC-type photodetectors offer a promising approach for sensitive and efficient light detection, with potential for further applications in solar energy conversion, environmental monitoring, and optoelectronic devices.

Recently, bismuth binary and mixed-anion compounds have been gradually used for the construction of PEC-type photodetectors.[79,147,149,217–224] The photodetection performance of bismuth binary and mixed-anion compound-based PEC-type photodetectors is summarized in Table 5. Remarkably, these photodetectors demonstrate a performance that is comparable to, and sometimes even superior to, the well-studied compound-based PEC-type photodetectors

Table 5 Photodetection performance of bismuth binary and mixed-anion compound-based PEC-type photodetectors

Sample	Fabrication method	Electrolyte	Light (nm)	Voltage (V)	R (mA W^{-1})	D^* (Jones)	τ_r/τ_d (ms)	Ref.
Bi_2O_3	Drop-casting	Polysulfide	365	0	29.92	7.46×10^{10}	20/70	224
	Template-assisted	Iodine electrolyte	365	0	1.01	7.79×10^{10}	28/40	217
Bi_2S_3	Liquid-phase exfoliation	0.1 M KOH	365	0.6	0.7	3.75×10^{8}	200/200	218
BiOI	Mist CVD	0.5 M Na_2SO_4 with 0.5 M Na_2SO_3	420	0	78.33	4.61×10^{11}	5/90	79
			520		28.89	1.68×10^{10}	—	
Bi_2O_2S	Drop-casting	1 M KOH	365	0	2.4	6.06×10^{9}	30/50	149
				0.6	13	2.34×10^{10}	10/45	
	Coating	0.5 M KOH	Sunlight	0.6	0.23	—	80/70	147
	Drop-casting	Solid-state	Sunlight	0	0.0102	—	45/13	219
	CBD	Iodine	850	0	9.48	9.96×10^{10}	27/47	221
Bi_2O_2Se	Drop-casting	1 M KOH	365	0	0.26	0.73×10^{8}	100/140	222
				0.6	0.68	2.44×10^{8}	85/103	
	Coating	Na_2SO_3	365	0	14.24	3.16×10^{8}	9/12	223
Bi_2O_2Se/graphene	Drop-casting	KOH/PVP	Xenon lamp	0	0.0065	—	400/310	225
Bi_2O_2S/GO	Drop-casting	KOH	Xenon lamp	0	0.035	4.5×10^{8}	420/2300	220
Bi_2S_3/Bi_2Se_3/Bi_2Te_3	CVD/PVD	0.1 M Na_2S + 0.02 M Na_2SO_3	475	−0.1	103	8.96×10^{9}	8/6.9	226
Bi_2S_3/MoS_2	CVD	0.1 M Na_2SO_3	420	0	0.218	—	4/15	227
Bi_2O_3/$CuBi_2O_4$	Sputtering	0.2 M K_2SO_4 + 0.2 M K_3PO_4 + H_2O_2	380	0	75	—	0.18/0.19	228

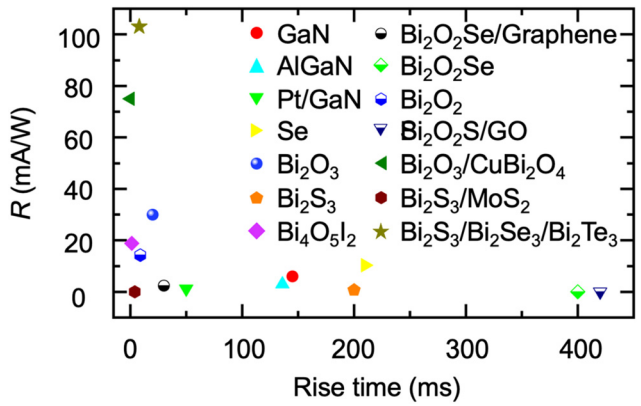

Fig. 12 Comparison of the photodetection performance of bismuth-based semiconductors and other well investigated PEC-type photodetectors.

(Fig. 12). They exhibit a broad spectral response, enabling light detection across a wide range of wavelengths. For instance, Bi_2O_2S has been reported to respond to light up to 850 nm, covering ultraviolet (UV) to infrared wavelengths, making it suitable for diverse applications.[149] Meanwhile, the low toxic and Earth-abundant nature of bismuth-based semiconductors endow it with possibilities for use in the construction of wearable devices.

Bismuth-based PEC-type photodetectors offered high photocurrent and photoresponsivity, indicating their ability to generate significant electrical signals in response to low-intensity light (Fig. 13a–c). The performance of bismuth-based PEC-type photodetectors was heavily dependent on the electrolyte composition (Fig. 13d). With the increase of electrolyte concentration, the interfacial resistance would decrease. The introduction of a hole scavenger to the electrolyte effectively promotes the separation of photogenerated electron–hole pairs, preventing the photodegradation of photoelectrodes.[79] For some cases, the electrolyte may react with the bismuth-based compound, leading to corrosion, degradation, or alterations in material properties, thus compromising the stability of the device.[229] Bismuth-based PEC-type photodetectors displayed fast response times, with rise and decay times in the microsecond order.[79,226–228] This rapid response is essential for real-time or high-speed light sensing and optical communications. These advantages make them highly appealing for large-scale manufacturing and integration into practical devices.

While bismuth-based compounds PEC-type photodetectors exhibited high responsivity, a broad-band range, and a rapid response time, the photoresponse stability deserved attention. To enhance the photoresponse stability, choosing a suitable electrolyte or applying a bias voltage is necessary.[79,149] Appling a voltage would lose the merits of self-powering so external electrics should be supplied. Adding a hole scavenger to the electrolyte or choosing a high-conductivity electrolyte can effectively improve the PEC-type photodetection stability, where the photogenerated holes can be promptly consumed by the hole scavenger.[79] However, with the increase in working time, the consumption would decrease the PEC photodetection performance.

The instability of bismuth-based compounds in the electrolyte is a major factor affecting the stability of PEC-type photo-

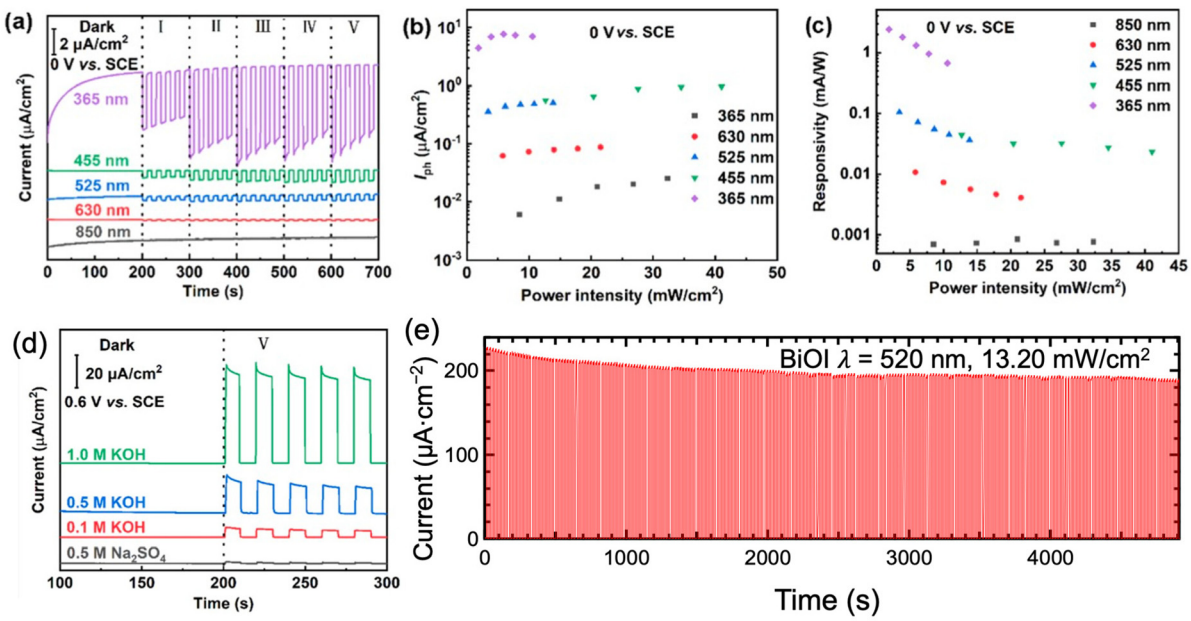

Fig. 13 (a) Current density, (b) I_{ph}, and (c) responsivity of Bi_2O_2S PEC-type photodetectors under the illumination of various wavelengths of light. (d) Effect of electrolytes on Bi_2O_2S PEC-type photodetectors. (e) Stability of BiOI PEC-type photodetectors. These figures have been adapted/reproduced from ref. 149 with permission from the American Chemical Society, copyright 2022 and from ref. 229 with permission from the American Chemical Society, copyright 2023.

detectors. Bismuth-based compounds undergo chemical reactions when exposed to harsh environmental conditions or prolonged light illumination, leading to degradation.[230] Additionally, uncontrolled charge carrier recombination at the surface or within the bismuth-based material can contribute to the deterioration of performance and stability in PEC-type photodetectors. This recombination process results in the loss of photoexcited charges before they can contribute to the photocurrent, diminishing the device's stability over time.[7,214,215] The packaging and protection of bismuth-based PEC-type photodetectors are vital for their long-term stability. Inadequate encapsulation or exposure to environmental factors, such as moisture or oxygen, can accelerate device degradation and impair stability. Furthermore, peeling off the thin films or nanoplates can also lead to a decrease in photodetection performance. Potential chemical degradation reactions affecting the stability of these compounds will be discussed later.

Addressing these stability challenges requires a comprehensive understanding and control over the material structure, device construction, and environmental conditions. Ongoing research should focus on developing strategies to mitigate these stability issues through interface engineering, material modifications, protective coatings, encapsulation techniques, and device architecture. These efforts aim to enhance the stability and durability of bismuth-based PEC-type photodetectors for practical applications in marine environments. Additionally, although the PEC performance of the bismuth-based compounds is comparable to the well-investigated compounds, there are few solar-blind photodetectors for the bismuth-based semiconductors, like GaN, which might be attributed to the relatively narrow bandgap.

4.2 PEC water splitting for H_2 generation

PEC water splitting is a kind of environmentally friendly, sustainable, and renewable technology to produce hydrogen energy. PEC water splitting in the sea holds significant importance from several aspects.[4,5] By harnessing the abundant solar energy available in marine environments, PEC water splitting can contribute to the production of clean hydrogen, benefiting both the marine industry and the broader energy sector. Meanwhile, PEC water splitting in the sea can contribute to reducing greenhouse gas emissions and marine pollution.[4,5] At present, PEC water splitting for H_2 generation in the sea mainly focuses on the following aspects:[2] (1) finding suitable sunlight absorption materials, and (2) optimization of the architecture of the photoelectrodes. By optimizing the configuration of the whole reaction system, including the optimization of the electrodes, the PEC performances can be much improved.

Currently, bismuth binary and mixed-anion compounds possess a high enough band level for H_2 (or O_2) production and a narrow band gap (<3.0 eV) for efficient visible light absorption.[13–15,20,24] It is indicated that the bismuth-based compounds discussed in this review showed great potential applications in H_2 generation, while there are no realistic applications.[13–15,20,24] Thus, this part just introduces PEC water splitting from the angle of laboratory experiments. For the bismuth binary and mixed-anion compounds in this review, most of them are n-type semiconductors. When the n-type bismuth-based semiconductor absorbed photons with energies higher than its own bandgap,[25,26] the photogenerated electrons moved to a counterelectrode, like Pt, used for the H_2 generation. Meanwhile, the holes migrate to the surface of the bismuth-based semiconductor and oxidize water to form O_2. To promote the efficient separation and transfer of the photogenerated carriers, an external electrical or chemical potential would be necessary to reduce the resistance at the electrode interfaces and within the solution. However, relying on a large external bias would result in high energy consumption.

Table 6 comprehensively summarized the recent PEC performance for the bare bismuth binary and mixed-anion compounds photoelectrodes. It can be summarized that the crystallinity, surface morphology, crystallographic orientation, and thickness would determine the PEC performance of bismuth-based semiconductor photoelectrodes. β-Bi_2O_3 thin film photoanodes with nanoporous surfaces showed better PEC activity at a bias of 0.197 V V_{NHE} than film photoanodes with dense surfaces.[157] Due to the nanoporous surface, the incident light reflected between the grains and electrolyte on the surface, rather than directly passing through the film, which significantly enhanced the photon absorption ability. However, to some extent, the very rough surface morphology would cause the recombination of electron holes at the boundary of the nanoplates.[231] However, it should be noted the relatively large bandgap for β-Bi_2O_3 was not efficient in absorbing the sunlight, leading to a moderate PEC performance among the bismuth binary and mixed-anion compounds.

For the Bi_2S_3, the deposition of continuous thin films is still very difficult, which limits the PEC performance. Meanwhile, the crystallinity influenced the photoresponse activity so that crystallized Bi_2S_3 thin films exhibited a much superior PEC performance to that of amorphous thin films.[181] In addition, the substrate would influence the PEC performance, and the observed photovoltage trend of the Bi_2S_3 electrodes (FTO > ITO > Mo > Au) inversely correlates with the Schottky barrier height at the Bi_2S_3 and substrate interface. FTO forms an ohmic contact, resulting in the smallest barrier height, which leads to the largest photovoltage and photocurrent. This trend suggests that the choice of electrode material significantly impacts the performance of Bi_2S_3-based photovoltaic devices.[183] Among the BiOX, BiOCl possessed a large bandgap higher than 3.0 eV, which is not suitable for harvesting solar light for the PEC applications.[195] In addition, due to the long transfer distance of charge carriers, excessively thick films can lead to electron–hole recombination.[196] As for the BiOBr and BiOI, there is a large number of reports confirming that BiOBr (Fig. 14a) exhibited better PEC performance than that of BiOI (Fig. 14b), although the BiOI possessed a stronger absorption ability for sunlight.[76] According to the calculation report, the large electron and hole mass for the BiOI would degrade the transfer and separation efficiency of

Table 6 PEC performance of previously reported bismuth binary and mixed-anion compound-based photoelectrodes

Sample	Format	Fabrication method	Bias voltage	Photocurrent density (μA cm^{-2})	Electrolyte	Light source	Ref.
Bi_2O_3	Thin film	Coating	1.23 V *vs.* RHE	1500	1 M Na_2SO_3	100 mW cm^{-2} Xe lamp	232
		CBD	1.23 V *vs.* RHE	480	K_2SO_4	100 mW cm^{-2} Xe lamp	233
		Electrochemical deposition	0.5 V *vs.* Ag/AgCl	970	1 M KOH	100 mW cm^{-2} Xe lamp	234
		Electrochemical deposition	0.5 V *vs.* Ag/AgCl	1000	0.5 M Na_2SO_4	100 mW cm^{-2} Xe lamp	46
		Chemical bath deposition	0.8 V *vs.* Ag/AgCl	300	0.1 M Na_2SO_4	35 mW cm^{-2} Xe lamp	235
Bi_2S_3	Nanosheet	Sputtering	1 V *vs.* Ag/AgCl	83	0.2 mol L^{-1} Na_2SO_4	100 W Xe lamp	179
	Thin film	Coating	1.23 V *vs.* RHE	2500	0.1 mol L^{-1} Na_2S and 0.1 mol L^{-1} Na_2SO_3	100 mW cm^{-2} Xe lamp	56
		Spin coating	0.3 V *vs.* Ag/AgCl	520	0.1 mol L^{-1} Na_2SO_3	50 mW cm^{-2} Xe lamp	184
		Chemical bath deposition	0 V *vs.* Ag/AgCl	125	Iodolyte AN-50	100 mW cm^{-2} Xe lamp	236
		SILAR	0.1 V *vs.* SCE	800	0.1 mol L^{-1} Na_2S	30 mW cm^{-2} Xe lamp	237
		Electrochemical deposition	1.23 V *vs.* RHE	9300	0.5 mol L^{-1} Na_2S	100 mW cm^{-2} Xe lamp	183
		Mist CVD	0.6 V *vs.* Ag/AgCl	2600	0.5 mol L^{-1} Na_2SO_3	30 mW cm^{-2} 420 nm LED light	181
BiOCl	Thin film	Dip-coating	0 V	0.05	0.1 mol L^{-1} Na_2SO_4	500 W Xe lamp	135
		Spin-coating	0 V	0.4	0.1 mol L^{-1} Na_2SO_4	300 W Xe lamp	238
		Mist CVD	−0.6 V *vs.* Ag/AgCl	2300	0.5 M Na_2SO_4 with 0.5 M Na_2SO_3	15.2 mW cm^{-2} 365 nm	195
BiOBr	Thin film	AACVD	1 V *vs.* Ag/AgCl	380	0.5 M Na_2SO_4	35 mW cm^{-2} Xe lamp	76
		Electrodeposition	0.2 V *vs.* RHE	200	0.5 M Na_2SO_4 + 50 mM KBr + 20 mM Br_2	375 W Hg quartz lamp	239
		Mist CVD	0.6 V *vs.* Ag/AgCl	330	0.5 M Na_2SO_4	50 mW cm^{-2} 420 nm	196
		CBD	0.9 V *vs.* Ag/AgCl	70	0.1 M Na_2SO_4	500 W Xe lamp	240
BiOI	Nanosheets	Chemical transformation	0.6 V *vs.* Ag/AgCl	6.5	0.5 mol L^{-1} Na_2SO_4	100 mW cm^{-2}	241
	Thin film	Solvothermal synthesis	0 V	10	0.1 mol L^{-1} Na_2SO_4	800	242
		Spray pyrolysis deposition	0.5 V	100	1 mol L^{-1} Na_2SO_4	100	197
		AACVD	0.5 V	*ca.* 80	0.5 mol L^{-1} Na_2SO_4	100	76
	(001) orientated thin film	Mist CVD	0 V	3	0.5 mol L^{-1} Na_2SO_4	70	79
			0.6 V	110			
	(102) orientated thin film		0 V	25			
			0.6 V	1360			
Bi_2O_2S	Thin film	Coating	0 V	2.5	0.5 M Na_2SO_4	300 W Xe lamp	243
Bi_2O_2Se	Nanosheet	Drop-casting	1.2 V	18	1 M Na_2SO_4	300 W Xe lamp	151

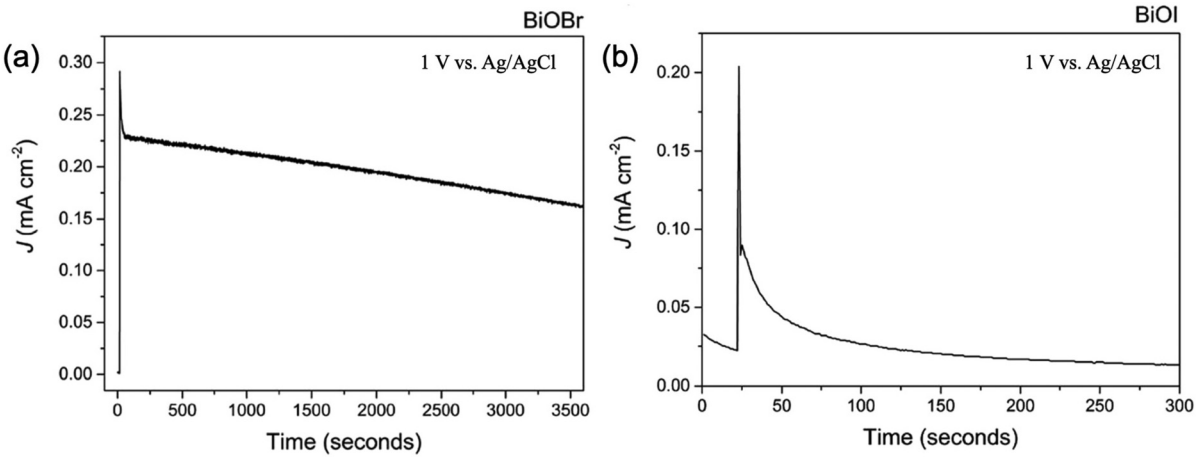

Fig. 14 The PEC stability of the (a) BiOBr and (b) BiOI thin film under illumination.[76] This figure was adapted from ref. 76 with permission from the Royal Society of Chemistry, copyright 2016.

photogenerated carriers. Prof. Carmalt's group demonstrated a preferred growth of the BiOBr film resulting in internal electric fields that minimized charge carrier recombination.[76] Recently, the effect of the crystallographic orientation on the PEC performance of BiOI was investigated. The intensive surface band bending and larger donor density for (102)-oriented BiOI effectively enhanced the charge separation and transfer.[79] However, as for the detailed mechanism, further investigation is necessary. Unlike other compounds, the investigation of Bi_2O_2S and Bi_2O_2Se in PEC water splitting is still at the early stage, which might be attributed to the immature thin films' deposition techniques. However, due to the narrower bandgap and high carrier mobility, it should exhibit a much more promising PEC performance.

Developing effective strategies to suppress electrode degradation, such as surface passivation or introducing appropriate heterojunctions, is essential for achieving high PEC performance. Efficient and durable catalysts are required on the surface of bismuth-based photoelectrodes to facilitate the water-splitting reactions. Although there are some reports on the heterostructure construction, doping, and modification of bismuth-based photoelectrodes, this review did not comment on this point in detail. However, nearly all the reports are on the format of nanoparticles.[13,14] As introduced in the above section, constructing photoelectrodes from nanoparticles *via* spin or dip coating is not an ideal method. Thus, exploring cost-effective synthesis methods and scalable manufacturing techniques is crucial to enable the widespread adoption of bismuth-based PEC devices.

In addition, the integration of "tandem" systems is a kind of promising strategy for enhancing PEC performance.[244] In a tandem configuration, one system includes a photoelectrode paired with a solar cell that provides the necessary external bias between the photoelectrode and the counterelectrode. The other system comprises an n-type semiconductor electrode alongside a suitable p-type semiconductor electrode. At the same time, these kinds of tandem device would also broaden the light absorption range. Very recently, $BiVO_4$–BiOI-based photoelectrodes exhibited a comparable PEC performance to that of the well-investigated photoelectrodes,[244] indicating the potential of bismuth-based semiconductors in PEC water splitting. Although the bismuth-based semiconductors did not exhibit much promising performance like other well-investigated compounds like Cu_2O and TiO_2, under continuous efforts from the point of innovative material design and advanced fabrication techniques, it is possible to realize the full potential of bismuth-based photoelectrodes in PEC applications.

3.3 Challenges and issues for PEC applications

PEC-type photodetection and water splitting based on bismuth binary and mixed-anion compounds showed promising potential in marine engineering. However, since 1990, the stability of bismuth-based compounds in electrolytes has attracted the attention of researchers.[245] Understanding the degradation mechanisms of bismuth-based photoelectrodes is critical for enhancing their stability and durability in PEC-type applications.

One degradation mechanism is photocorrosion, where electrochemical reactions occurred within the material under light illumination, leading to its deterioration. Photocorrosion involves reduction, dissolution, or the formation of self-passivating surface layers.[197] Additionally, bismuth-based photoelectrodes undergo surface oxidation in the presence of oxygen or water.[197] Another factor contributing to degradation is rapid electron–hole recombination within the bismuth-based material. This recombination process hampers the charge separation efficiency, resulting in a reduced photocurrent and overall photoelectrode performance.[76] Previous reports suggest that changing the electrolytes, with or without hole scavengers like Na_2SO_3, simplifies the degradation mechanism.[195] If electrons cannot be promptly consumed, photogenerated electrons may reduce Bi^{3+} into Bi (0) following the equation:

$$BiOX + 2H^+ + 3e^- \rightarrow Bi + X^- + H_2O$$

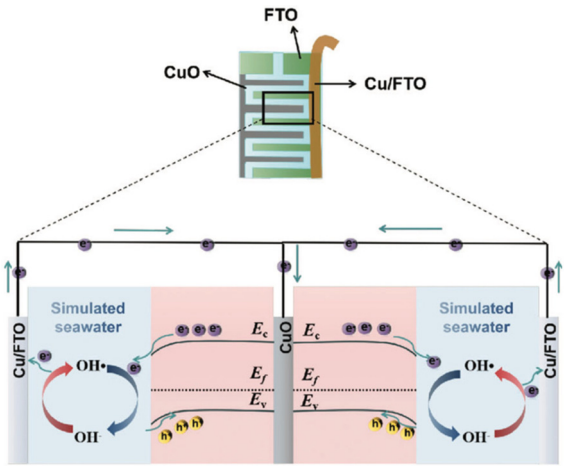

Fig. 15 Setup of the planar interdigital photoelectrodes.[246] This figure was adapted from ref. 246 with permission from Wiley, copyright 2024.

Furthermore, the marine environment introduces additional challenges such as salt and humidity, which can affect the corrosion resistance of materials. Bismuth-based semiconductors must exhibit excellent corrosion resistance to ensure prolonged stable operation. Further research and exploration are necessary to overcome these challenges and promote the application of bismuth-based semiconductors in marine engineering. In conclusion, addressing the stability and durability of bismuth-based photoelectrodes is crucial for their successful deployment in PEC-type applications, including those in the marine environment.

5. Prospects and outlook of recent advances

5.1 Optimization of electrode architecture

To some extent, bismuth binary and mixed-anion compounds for PEC-type device construction were underexplored for a long time owing to the not good stability. Very recently, Andrei and coworkers confirmed that bismuth-based semiconductor BiOI–$BiVO_4$ tandem photoelectrodes can approach and even challenge the performance of well-established light absorbers with an appropriate device architecture.[244] In this work, the p-type amorphous NiO_x and n-type ZnO were used as a hole transport and electron layer respectively, and graphite composite epoxy was used as a conductive encapsulator to improve the transfer and separation efficiency of photogenerated electron–hole pairs. In addition, multiple-pixel devices were found that would be useful in overcoming the current leakage in the grain boundary and defects of thin films.[244]

In addition, Feng proposed the planar interdigital photoelectrode structure (Fig. 15), which has been successfully applied in p-Se and CuSe PEC-type photodetectors, showing various advantages, like a simplified design and excellent photoresponse.[246] The planar interdigital photoelectrode structure offers a novel approach to the development of high-performance, cost-effective, photoelectrodes.[246] Shortly, further optimization of the lateral and vertical structure would be necessary for the enhancement of the PEC performance of conventional PEC-type devices.

5.2 Fabrication of freestanding membranes

Freestanding membranes, also known as self-supporting membranes, are thin, flexible structures or films that are capable of standing or existing independently without the need for additional external support.[247] Freestanding membranes are typically thin and flexible, allowing them to conform to different shapes and surfaces. This flexibility enables their integration into complex structures or devices, making them suitable for applications that require conformable materials. Meanwhile, the freestanding membranes are free of solid-state bulk substrates like single crystal and glass substrates, which effectively reduce the cost and weight.[248] Importantly, freestanding membranes minimize interfacial effects between the membrane and the supporting substrate. This allows for a more accurate characterization of intrinsic membrane properties and mitigates potential limitations associated with interfacial interactions, such as diffusion barriers or catalytic effects.[249,250]

Currently, there are nearly no reports on bismuth-based binary and mixed-anion compound freestanding membranes, while there are several reports on the exfoliation and transfer of Bi_2O_2Se nanoplates.[208,209] Thus, future research should be devoted to the perspective of selecting suitable substrates, and optimization of exploitation-transfer techniques. Coupling the freestanding membranes with flexible organic conduction layers will be suitable for practical PEC device construction with low cost and weight, better flexibility, and enhanced PEC performance. In addition, the successful fabrication of freestanding membranes would promote the investigation of intrinsic properties and enhancement of transfer and separation efficiency of photogenerated electron–hole pairs. Advances in material science and manufacturing techniques should continue to expand the capabilities and explore new applications for freestanding membranes. Freestanding membranes offer a versatile platform for various applications like flexible smart devices.

5.3 Underwater communication through PEC-type photodetectors

PEC-type photodetectors can play a crucial role in underwater communication systems by enabling the wireless transmission of data using light.[7] PEC-type photodetectors excel at detecting light signals and converting them into electrical signals. In wireless communication, these devices can receive optical signals carrying information and convert them into electrical signals that can be processed by electronic systems. PEC-type photodetectors can be integrated into optical communication systems to receive data encoded in optical signals (Fig. 16).[216] For instance, in free-space optical communication or optical wireless communication, PEC-type photodetectors can detect modulated light signals, such as those from laser diodes or light-emitting diodes (LEDs), and convert them into electrical

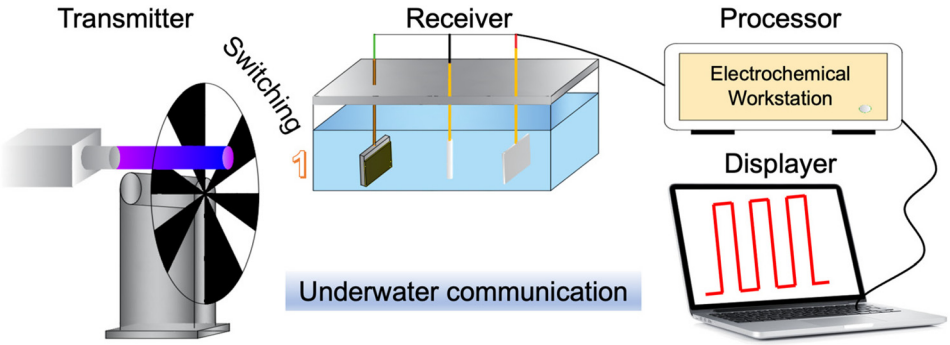

Fig. 16 The schematic diagram for the underwater optical communication system.[216] This figure was adapted with permission from Wiley, copyright 2024.

signals for further processing. As depicted in section 4.1, the PEC-type photodetectors constructed from the bismuth binary and mixed-anion compounds can operate with self-powered, high-photoresponse speeds, excellent sensitivity, and a broad photoresponse to light signals, making them suitable for applications such as wireless communication links between remote locations, the transmission of data at high speeds, and supporting a large data transfer capacity.[216] However, the development of PEC-type photodetectors in the field of underwater communication is still at an early stage. Shortly, the PEC-type photodetectors can be paired with other electronic and optical components, like optical transmitters, to establish a complete wireless underwater communication link, allowing for bidirectional communication.

5.4 Finding novel mixed-anion compounds

Bismuth-based binary and mixed-anion compounds have been regarded as a kind of important functional material due to their various extraordinary properties, like the tunable bandgap and ultrahigh carrier mobility.[251] In the past decades, the investigation of bismuth-based binary and mixed-anion compounds was mainly focused on simple ternary compounds like bismuth oxyhalides,[14] though slightly changing the chemical composition would bring unprecedented properties. For instance, despite the similar Bi : S molar ratio and crystal structure for Bi_2S_3 and $Bi_{13}S_{18}I_2$, the bandgap of $Bi_{13}S_{18}I_2$ (0.8 eV)[252] was much narrower than that of Bi_2S_3 (1.3 eV).[181] Benefiting from the narrow bandgap, $Bi_{13}S_{18}I_2$ attracted much attention for various applications, like solar cells, photoelectrodes, and photodetectors.[253–255] Thus, for fruitful applications of bismuth-based binary and mixed-anion compounds, controlling the anion composition would be a promising way to optimize the physical and chemical properties of bismuth-based compounds to meet the high demand of PEC-type device construction.

In addition, doping elements, introducing oxygen vacancies, and constructing heterostructures can significantly enhance the PEC performance of bismuth-based compounds.[256] Most of the previously published reports on bismuth-based compounds have focused on nanoparticles. Achieving modifications in the format of thin films remains challenging, and this can be attributed to the immaturity of deposition techniques for thin film fabrication. Despite these challenges, the modification of bismuth-based compounds holds promise for improving their properties and expanding their potential applications in PEC systems. Efforts in research and development are necessary to overcome the current limitations and fully unlock the potential of bismuth-based compounds. Progress in materials synthesis techniques, especially in developing reliable methods for thin film deposition, will be essential to advance the modification of bismuth-based compounds for practical applications. Continued research is vital to address these challenges and achieve the desired improvements in the properties and performance of bismuth-based compounds.

5.5 Challenges for practical applications in marine engineering

PEC-type devices based on bismuth-based compounds hold great potential for practical applications in marine engineering. However, there are several challenges associated with PEC activities in marine environments. One of the main challenges is corrosion. Marine environments are highly corrosive due to the presence of salts, minerals, and other impurities in seawater. Therefore, PEC materials and electrodes used in water splitting systems must be corrosion-resistant to ensure long-term performance and durability. Another challenge is fouling. Marine environments are prone to fouling, where organisms such as algae, barnacles, and mussels attach and grow on the surfaces of PEC systems. This can hinder water flow and reduce the efficiency of light absorption, leading to decreased performance and increased maintenance requirements. Moreover, seawater has higher light absorption and scattering properties compared with freshwater or air, which can further reduce the efficiency of light absorption in PEC systems. As mentioned above, the stability and durability of bismuth-based materials in marine environments are also crucial for their practical applications. Research and development efforts are required to improve the stability and durability of these materials under marine conditions. Lastly, the manufacturing, installation, and maintenance of large-scale PEC systems in marine environments require significant

investments and infrastructure. Future research should focus on improving the corrosion resistance, anti-fouling properties, light absorption, stability, and cost-effectiveness of PEC materials and systems in marine engineering applications.

6. Conclusion

This review initially discusses the crystal structure and intrinsic properties of bismuth binary and mixed-anion compounds. Their excellent optical and electrical properties make them promising candidates for potential applications in marine environments. Currently, PEC-type devices based on bismuth binary and mixed-anion compounds can effectively harness photon energy and perform various functions in marine engineering, such as hydrogen production and photodetection. However, it is important to recognize that further research and development are required to optimize the performance and stability of bismuth-based PEC devices for marine engineering applications. While the application of bismuth optoelectronic semiconductor materials in marine engineering is still in the research stage, the deepening exploration of marine spaces will unveil the unique advantages of bismuth-based semiconductor materials in multiple scenarios, including underwater communication, desalination and water treatment, corrosion protection, and environmental monitoring. Meanwhile, these materials can contribute to realize the zero carbon and smart ocean.

Author contributions

Jiaji Zhang and Zaichun Sun conceived this review. All authors did the literature survey, wrote the manuscript, and commented on the paper. All authors have approved the final version of this manuscript.

Conflicts of interest

The authors declare no competing financial interests.

Acknowledgements

This work was supported by the National Natural Science Foundation of China (No. 52272161), Key R&D Project of Hainan Yourui Cohesion Technology Co., Ltd (20231201ZZKY002), Wuhan Key R&D Plan (2023020402010590), and Fundamental Research Funds for the Central Universities (WUT: 2024IVA007). We thank Mr Yao Chen, Guoxiao Zhao, Qinna Ren, and Weibojie Lu for their assistance in the literature survey.

References

1 R. Tang, S. Zhou, Z. Zhang, R. Zheng and J. Huang, *Adv. Mater.*, 2021, **33**, 2005389.
2 A. Vilanova, P. Dias, T. Lopes and A. Mendes, *Chem. Soc. Rev.*, 2024, **53**, 2388–2434.
3 C. S. Gopinath and N. Nalajala, *J. Mater. Chem. A*, 2021, **9**, 1353–1371.
4 X. Zeng, Y. Liu, X. Hu and X. Zhang, *Green Chem.*, 2021, **23**, 1466–1494.
5 N. S. Lewis, *Science*, 2016, **351**, 353.
6 Y. Ding, S. Maitra, C. Wang, S. Halder, R. Zheng, T. Barakat, S. Roy, L. Chen and B. Su, *Interdiscip. Mater.*, 2022, **1**, 213–255.
7 H. Qiao, Z. Huang, X. Ren, S. Liu, Y. Zhang, X. Qi and H. Zhang, *Adv. Opt. Mater.*, 2020, **8**, 1900765.
8 J. Gao, X. Yao, Y. Chen, Z. Gao and J. Zhang, *Anal. Chem.*, 2021, **93**, 677–682.
9 K. Fujishima and A. Honda, *Nature*, 1972, **238**, 38–40.
10 C. Ros, T. Andreu and J. R. Morante, *J. Mater. Chem. A*, 2020, **8**, 10625–10669.
11 R. Siavash Moakhar, S. M. Hosseini-Hosseinabad, S. Masudy-Panah, A. Seza, M. Jalali, H. Fallah-Arani, F. Dabir, S. Gholipour, Y. Abdi, M. Bagheri-Hariri, N. Riahi-Noori, Y. F. Lim, A. Hagfeldt and M. Saliba, *Adv. Mater.*, 2021, **33**, 2007285.
12 R. Gao and D. Yan, *Adv. Energy Mater.*, 2020, **10**, 1900954.
13 S. Wang, L. Wang and W. Huang, *J. Mater. Chem. A*, 2020, **8**, 24307–24352.
14 X. Wu, C. Y. Toe, C. Su, Y. H. Ng, R. Amal and J. Scott, *J. Mater. Chem. A*, 2020, **8**, 15302–15318.
15 A. Zhao, L. Zhang, Y. Guo, H. Li, S. Ruan and Y. J. Zeng, *2D Mater.*, 2021, **8**, 012004.
16 K. Hoshi and Y. Mizuguchi, *J. Phys.: Condens. Matter*, 2021, **33**, 473001.
17 J. He, X. Hu, Z. Liu, W. Chen and G. Longo, *Adv. Funct. Mater.*, 2023, **33**, 2306075.
18 R. Mohan, *Nat. Chem.*, 2010, **2**, 336.
19 A. Walsh, D. J. Payne, R. G. Egdell and G. W. Watson, *Chem. Soc. Rev.*, 2011, **40**, 4455–4463.
20 X. Meng and Z. Zhang, *J. Mol. Catal. A: Chem.*, 2016, **423**, 533–549.
21 J. Di, J. Xia, H. Li, S. Guo and S. Dai, *Nano Energy*, 2017, **41**, 172–192.
22 N. C. Miller and M. Bernechea, *APL Mater.*, 2018, **6**, 084503.
23 P. Xia, Y. J. Song, Y. Z. Liu, M. X. Long, C. Yang, X. Y. Zhang and T. Zhang, *J. Mater. Chem. C*, 2023, **12**, 1609–1624.
24 L. Ye, Y. Deng, L. Wang, H. Xie and F. Su, *ChemSusChem*, 2019, **12**, 3671–3701.
25 Z. Ran, X. Wang, Y. Li, D. Yang, X. G. Zhao, K. Biswas, D. J. Singh and L. Zhang, *npj Comput. Mater.*, 2018, **4**, 1–7.
26 E. Wlaźlak, A. Blachecki, M. Bisztyga-Szklarz, S. Klejna, T. Mazur, K. Mech, K. Pilarczyk, D. Przyczyna, M. Suchecki, P. Zawal and K. Szaciłowski, *Chem. Commun.*, 2018, **54**, 12133–12162.
27 J. Wu, H. Yuan, M. Meng, C. Chen, Y. Sun, Z. Chen, W. Dang, C. Tan, Y. Liu, J. Yin, Y. Zhou, S. Huang,

H. Q. Xu, Y. Cui, H. Y. Hwang, Z. Liu, Y. Chen, B. Yan and H. Peng, *Nat. Nanotechnol.*, 2017, **12**, 530–534.
28 R. L. Z. Hoye, L. C. Lee, R. C. Kurchin, T. N. Huq, K. H. L. Zhang, M. Sponseller, L. Nienhaus, R. E. Brandt, J. Jean, J. A. Polizzotti, A. Kursumović, M. G. Bawendi, V. Bulović, V. Stevanović, T. Buonassisi and J. L. MacManus-Driscoll, *Adv. Mater.*, 2017, **29**, 1702176.
29 M. Wu, Z. Lou, C. M. Dai, T. Wang, J. Wang, Z. Zhu, Z. Xu, T. Sun, W. Li, X. Zheng and X. Lin, *Adv. Mater.*, 2023, **35**, 2300450.
30 T. Ghosh, M. Samanta, A. Vasdev, K. Dolui, J. Ghatak, T. Das, G. Sheet and K. Biswas, *Nano Lett.*, 2019, **19**, 5703–5709.
31 S. Abhirami, E. P. Amaladass, S. Amirthapandian, C. David and A. Mani, *Phys. Chem. Chem. Phys.*, 2023, **26**, 2745–2767.
32 M. Channegowda, R. Mulla, Y. Nagaraj, S. Lokesh, S. Nayak, S. Mudhulu, C. K. Rastogi, C. W. Dunnill, H. K. Rajan and A. Khosla, *ACS Appl. Energy Mater.*, 2022, **5**, 7913–7943.
33 C. Yang, Y. Zhao, P. Liu, D. Wang, Y. Sun, C. Li, Y. Dong, M. Ye, N. Zhang, Z. Zhu, H. Jiang, J. Zhu, M. Shuai, T. Wei and Y. Zhao, *Cryst. Res. Technol.*, 2023, **58**, 2300081.
34 M. Sahu and C. Park, *Mater. Today Sustain.*, 2023, **23**, 100441.
35 X. Wang, B. Liu, Y. Zhang, T. Butburee, K. (Ken) Ostrikov, S. Wang and W. Huang, *EcoEnergy*, 2023, **1**, 108–153.
36 Y. Zhang, L. Xu, B. Liu, X. Wang, T. Wang, X. Xiao, S. Wang and W. Huang, *ACS Catal.*, 2023, **13**, 5938–5948.
37 S. Wang, T. He, J. H. Yun, Y. Hu, M. Xiao, A. Du and L. Wang, *Adv. Funct. Mater.*, 2018, **28**, 1802685.
38 B. Guan, J. Chen, Z. Li, Z. Zhuang, Y. Chen, Z. Ma, J. Guo, C. Zhu, X. Hu, S. Zhao, H. Dang, L. Chen, K. Shu, Z. Guo, K. Shi, Y. Li, C. Yi, J. Hu and Z. Huang, *Energy Fuels*, 2024, **38**, 806–853.
39 S. Wang, X. Wang, B. Liu, Z. Guo, K. Ostrikov, L. Wang and W. Huang, *Nanoscale*, 2021, **13**, 17989–18009.
40 A. H. Zahid and Q. Han, *Nanoscale*, 2021, **13**, 17687–17724.
41 F. K. Wang, S. J. Yang and T. Y. Zhai, *iScience*, 2021, **24**, 103291.
42 P. Ngabonziza, *Nanotechnology*, 2022, **33**, 192001.
43 X. Tang, Z. Li, W. Liu, Q. Zhang and C. Uher, *Interdiscip. Mater.*, 2022, **1**, 88–115.
44 A. J. Lovett, M. P. Wells, Z. He, J. Lu, H. Wang and J. L. Macmanus-Driscoll, *J. Mater. Chem. A*, 2022, **10**, 3478–3484.
45 D. Pérez-Mezcua, I. Bretos, R. Jiménez, J. Ricote, R. J. Jiménez-Rioboó, C. G. Da Silva, D. Chateigner, L. Fuentes-Cobas, R. Sirera and M. L. Calzada, *Sci. Rep.*, 2016, **6**, 39561.
46 M. W. Kim, B. Joshi, E. Samuel, K. Kim, Y. Il Kim, T. G. Kim, M. T. Swihart and S. S. Yoon, *J. Alloys Compd.*, 2018, **764**, 881–889.
47 Y. Li, J. Song, Y. Ji, X. Lu, Q. Tian, J. Chen and Z. Sui, *J. Phys. Chem. Solids*, 2022, **163**, 110562.
48 Z. Wu, M. C. Chong, S. Zhang, J. Li and Y. Zhu, *Sci. China: Chem.*, 2024, DOI: **10.1007/s11426-023-1943-5**.
49 B. Wu, Z. Su, Q. Wu, D. H. Kuo, P. Zhang, L. Chen, A. B. Abdeta, M. T. Mosisa, J. Lin, X. Chen and X. Liu, *Mater. Today Chem.*, 2023, **33**, 101697.
50 Z. Zhu, S. K. Iyemperumal, K. Kushnir, A. D. Carl, L. Zhou, D. R. Brodeur, R. L. Grimm, L. V. Titova, N. A. Deskins and P. M. Rao, *Sustainable Energy Fuels*, 2017, **1**, 2134–2144.
51 P. S. Sonawane and L. A. Patil, *Mater. Chem. Phys.*, 2007, **105**, 157–161.
52 Z. Hu, D. Zhao, Y. Li, X. Lv, J. Song, L. Meng, S. Y. Lien and P. Gao, *ACS Mater. Lett.*, 2023, **5**, 2987–2999.
53 M. Bernechea, Y. Cao and G. Konstantatos, *J. Mater. Chem. A*, 2015, **3**, 20642–20648.
54 M. Zargazi and M. H. Entezari, *J. Hazard. Mater.*, 2020, **384**, 121300.
55 L. Zhao, J. Zhou, L. Zhang, X. Sun, X. Sun, T. Yan, X. Ren and Q. Wei, *ACS Appl. Mater. Interfaces*, 2020, **12**, 55838–55843.
56 P. Subramanyam, T. Vinodkumar, M. Deepa and C. Subrahmanyam, *J. Mater. Chem. C*, 2019, **7**, 6398–6405.
57 M. F. Afsar, M. A. Rafiq, A. Jamil, S. Fareed, F. Siddique, A. I. Y. Tok and M. M. U. Hasan, *ACS Omega*, 2019, **4**, 2030–2039.
58 W. Yang, J. Yang, K. Zhao, Q. Gao, L. Liu, Z. Zhou, S. Hou, X. Wang, G. Shen, X. Pang, Q. Xu and Z. Wei, *Adv. Sci.*, 2021, **8**, 2100075.
59 Y. Hu, L. Mao, X. Yuan, J. Lu, R. Chen, T. Chen, W. Zhang, X. Xue, W. Yan, M. Shokouhimehr, X. L. Zhang and Z. Jin, *Nano Res.*, 2020, **13**, 2226–2232.
60 N. Huo, A. Figueroba, Y. Yang, S. Christodoulou, A. Stavrinadis, C. Magén and G. Konstantatos, *Adv. Opt. Mater.*, 2019, **7**, 1900258.
61 P. Rong, S. Gao, S. Ren, H. Lu, J. Yan, L. Li, M. Zhang, Y. Han, S. Jiao and J. Wang, *Adv. Funct. Mater.*, 2023, **33**, 2300159.
62 Y. Zhao, L. Ma, Y. Zhu, P. Qin, H. Li, F. Mo, D. Wang, G. Liang, Q. Yang, W. Liu and C. Zhi, *ACS Nano*, 2019, **13**, 7270–7280.
63 B. Long, Z. Qiao, J. Zhang, S. Zhang, M. S. Balogun, J. Lu, S. Song and Y. Tong, *J. Mater. Chem. A*, 2019, **7**, 11370–11378.
64 J. Jiang, X. Che, Y. Qian, L. Wang, Y. Zhang and Z. Wang, *Front. Mater.*, 2020, **7**, 234.
65 J. Guo, J. Yang, Z. Ge, B. Jiang, Y. Qiu, Y. Zhu and X. Wang, *Adv. Funct. Mater.*, 2021, **12**, 202102838.
66 S. Sharma, H. H. Singh, S. Kumar and N. Khare, *Nanotechnology*, 2021, **32**, 335705.
67 J. Yang, Y. Xue, C. Han, X. Zhang, K. Sa, J. Jia, H. Ye and Y. Liang, *Catal. Sci. Technol.*, 2023, **13**, 5313–5325.
68 X. D. Dong, Y. M. Zhang and Z. Y. Zhao, *Inorg. Chem.*, 2021, **60**, 8461–8474.
69 S. Rieger, T. Fürmann, J. K. Stolarczyk and J. Feldmann, *Nano Lett.*, 2021, **21**, 7887–7893.
70 T. Li, X. Zhang, C. Zhang, R. Li, J. Liu, R. Lv, H. Zhang, P. Han, C. Fan and Z. Zheng, *Phys. Chem. Chem. Phys.*, 2019, **21**, 868–875.

71 D. Kato, K. Hongo, R. Maezono, M. Higashi, H. Kunioku, M. Yabuuchi, H. Suzuki, H. Okajima, C. Zhong, K. Nakano, R. Abe and H. Kageyama, *J. Am. Chem. Soc.*, 2017, **139**, 18725–18731.
72 L. S. Gómez-Velázquez, A. Hernández-Gordillo, M. J. Robinson, V. J. Leppert, S. E. Rodil and M. Bizarro, *Dalton Trans.*, 2018, **47**, 12459–12467.
73 A. M. Ganose, M. Cuff, K. T. Butler, A. Walsh and D. O. Scanlon, *Chem. Mater.*, 2016, **28**, 1980–1984.
74 W. L. Huang and Q. Zhu, *Comput. Mater. Sci.*, 2009, **46**, 1076–1084.
75 H. Zhang, L. Liu and Z. Zhou, *RSC Adv.*, 2012, **2**, 9224–9229.
76 D. S. Bhachu, S. J. A. Moniz, S. Sathasivam, D. O. Scanlon, A. Walsh, S. M. Bawaked, M. Mokhtar, A. Y. Obaid, I. P. Parkin, J. Tang and C. J. Carmalt, *Chem. Sci.*, 2016, **7**, 4832–4841.
77 R. A. Jagt, T. N. Huq, K. M. Börsig, D. Sauven, L. C. Lee, J. L. Macmanus-Driscoll and R. L. Z. Hoye, *J. Mater. Chem. C*, 2020, **8**, 10791–10797.
78 M. Shi, G. Li, J. Li, X. Jin, X. Tao, B. Zeng, E. A. Pidko, R. Li and C. Li, *Angew. Chem., Int. Ed.*, 2020, **59**, 6590–6595.
79 Z. Sun, H. Zhang and B. Mei, *Inorg. Chem.*, 2023, **62**, 5512–5519.
80 W. Zeng, J. Li, L. Feng, H. Pan, X. Zhang, H. Sun and Z. Liu, *Adv. Funct. Mater.*, 2019, **29**, 1900129.
81 B. S. Defects, T. N. Huq, L. C. Lee, L. Eyre, W. Li, R. A. Jagt, C. Kim, S. Fearn, V. Pecunia, F. Deschler, J. L. Macmanus-driscoll and R. L. Z. Hoye, *Adv. Funct. Mater.*, 2020, **11**, 1909983.
82 R. A. Jagt, I. Bravić, L. Eyre, K. Gałkowski, J. Borowiec, K. R. Dudipala, M. Baranowski, M. Dyksik, T. W. J. van de Goor, T. Kreouzis, M. Xiao, A. Bevan, P. Płochocka, S. D. Stranks, F. Deschler, B. Monserrat, J. L. MacManus-Driscoll and R. L. Z. Hoye, *Nat. Commun.*, 2023, **14**, 1–12.
83 C. Gong, J. Chu, S. Qian, C. Yin, X. Hu, H. Wang, Y. Wang, X. Ding, S. Jiang, A. Li, Y. Gong, X. Wang, C. Li, T. Zhai and J. Xiong, *Adv. Mater.*, 2020, **32**, 1908242.
84 C. Wang, C. Hu, F. Chen, H. Li, Y. Zhang, T. Ma and H. Huang, *Adv. Funct. Mater.*, 2023, **33**, 2301144.
85 P. Lei, H. Duan, L. Qin, X. Wei, R. Tao, Z. Wang, F. Guo, M. Song, W. Jie and J. Hao, *Adv. Funct. Mater.*, 2022, **32**, 2201276.
86 T. Li and H. Peng, *Acc. Mater. Res.*, 2021, **2**, 842–853.
87 M. Wu and X. C. Zeng, *Nano Lett.*, 2017, **17**, 6309–6314.
88 Y. Sun, J. Zhang, S. Ye, J. Song and J. Qu, *Adv. Funct. Mater.*, 2020, **30**, 2004480.
89 F. Wang, S. Yang, J. Wu, X. Hu, Y. Li, H. Li, X. Liu, J. Luo and T. Zhai, *InfoMat*, 2021, **3**, 1251–1271.
90 Y. Liang, X. Zhou, W. Li and H. Peng, *APL Mater.*, 2021, **9**, 060905.
91 J. Wu, C. Qiu, H. Fu, S. Chen, C. Zhang, Z. Dou, C. Tan, T. Tu, T. Li, Y. Zhang, Z. Zhang, L. M. Peng, P. Gao, B. Yan and H. Peng, *Nano Lett.*, 2019, **19**, 197–202.
92 J. Wu, H. Yuan, M. Meng, C. Chen, Y. Sun, Z. Chen, W. Dang, C. Tan, Y. Liu, J. Yin, Y. Zhou, S. Huang, H. Q. Xu, Y. Cui, H. Y. Hwang, Z. Liu, Y. Chen, B. Yan and H. Peng, *Nat. Nanotechnol.*, 2017, **12**, 530–534.
93 Z. Guan, H. Hu, X. Shen, P. Xiang, N. Zhong, J. Chu and C. Duan, *Adv. Electron. Mater.*, 2020, **6**, 1900818.
94 M. T. Hossain, T. Jena and P. K. Giri, *Small Struct.*, 2024, **5**, 2300511.
95 H. Guo, J. Xiao, J. Qu, D. Legut and Q. Zhang, *J. Phys. Chem. C*, 2019, **123**, 24024–24030.
96 C. W. Hu, Y. Yang, C. Hou and T. X. Liang, *Mater. Today Commun.*, 2020, **25**, 101619.
97 H. Tang, B. Shi, Y. Wang, C. Yang, S. Liu, Y. Li, R. Quhe and J. Lu, *Phys. Rev. Appl.*, 2021, **15**, 1.
98 Q. Wei, C. Lin, Y. Li, X. Zhang, Q. Zhang, Q. Shen, Y. Cheng and W. Huang, *J. Appl. Phys.*, 2018, **124**, 055701.
99 T. Cheng, C. Tan, S. Zhang, T. Tu, H. Peng and Z. Liu, *J. Phys. Chem. C*, 2018, **122**, 19970–19980.
100 H. Y. Song, X. J. Ge, M. Y. Shang, J. Zhang and J. T. Lü, *Phys. Chem. Chem. Phys.*, 2019, **21**, 18259–18264.
101 C. Zhang, J. Wu, Y. Sun, C. Tan, T. Li, T. Tu, Y. Zhang, Y. Liang, X. Zhou, P. Gao and H. Peng, *J. Am. Chem. Soc.*, 2020, **142**, 2726–2731.
102 H. Tao, T. Wang, D. Li, J. Xing and G. Li, *J. Semicond.*, 2023, **44**, 031001.
103 C. Tan, S. Xu, Z. Tan, L. Sun, J. Wu, T. Li and H. Peng, *InfoMat*, 2019, **1**, 390–395.
104 W. Chen, R. Zhang, Y. Sun, J. Wang, Y. Fan and B. Liu, *Adv. Powder Mater.*, 2023, **2**, 100080.
105 Y. Chen, W. Ma, C. Tan, M. Luo, W. Zhou, N. Yao, H. Wang, L. Zhang, T. Xu, T. Tong, Y. Zhou, Y. Xu, C. Yu, C. Shan, H. Peng, F. Yue, P. Wang, Z. Huang and W. Hu, *Adv. Funct. Mater.*, 2021, **31**, 202009554.
106 P. Luo, F. Wang, J. Qu, K. Liu, X. Hu, K. Liu and T. Zhai, *Adv. Funct. Mater.*, 2021, **31**, 202008351.
107 J. Li, Z. Wang, J. Chu, Z. Cheng, P. He, J. Wang, L. Yin, R. Cheng, N. Li, Y. Wen and J. He, *Appl. Phys. Lett.*, 2019, **114**, 5094192.
108 M. Yu, C. Fang, J. Han, W. Liu, S. Gao and K. Huang, *ACS Appl. Mater. Interfaces*, 2022, **14**, 13507–13515.
109 H. Yang, C. Tan, C. Deng, R. Zhang, X. Zheng, X. Zhang, Y. Hu, X. Guo, G. Wang, T. Jiang, Y. Zhang, G. Peng, H. Peng, X. Zhang and S. Qin, *Small*, 2019, **15**, 201904482.
110 L. Pan, X. L. Shi, C. Song, W. Di Liu, Q. Sun, C. Lu, Q. Liu, Y. Wang and Z. G. Chen, *Adv. Funct. Mater.*, 2022, **32**, 202202927.
111 W. Ai, J. Chen, X. Dong, Z. Gao, Y. He, Z. Liu, H. Fu, F. Luo and J. Wu, *Nano Lett.*, 2022, **22**, 7659–7666.
112 Y. Yan, Y. Xu, S. Lei, X. Ou, L. Chen, J. Xiong, Y. Xiao and B. Cheng, *Dalton Trans.*, 2018, **47**, 3408–3416.
113 J. Tang, T. Zhang, Z. Duan, C. Li, C. Meng, Y. Zhang, Q. Zhang, D. Hou, Q. Xv and Y. Zhu, *Chem. Phys. Lett.*, 2021, **768**, 138354.
114 V. G. Ilves, V. S. Gaviko, A. M. Murzakaev, S. Y. Sokovnin, M. A. Uimin and M. G. Zuev, *Ceram. Int.*, 2023, **49**, 21848–21854.

115 P. Guo, F. Yin, J. Zhang, B. Chen, Z. Ni, L. Shi, M. Han, Z. Wu and G. Li, *ACS Appl. Mater. Interfaces*, 2024, **16**, 17540–17552.
116 Y. C. Liang and K. W. Liang, *CrystEngComm*, 2023, **25**, 5035–5049.
117 Y. Lu, Y. Zhao, J. Zhao, Y. Song, Z. Huang, F. Gao, N. Li and Y. Li, *Cryst. Growth Des.*, 2015, **15**, 1031–1042.
118 M. Weber, M. Schlesinger and M. Mehring, *Cryst. Growth Des.*, 2016, **16**, 5678–5688.
119 T. Selvamani, S. Anandan, L. Granone, D. W. Bahnemann and M. Ashokkumar, *Mater. Chem. Front.*, 2018, **2**, 1664–1673.
120 M. Schlesinger, S. Schulze, M. Hietschold and M. Mehring, *Dalton Trans.*, 2013, **42**, 1047–1056.
121 H. W. Kim, J. W. Lee and C. Lee, *J. Korean Phys. Soc.*, 2007, **50**, 1308–1311.
122 Y. Qiu, D. Liu, J. Yang and S. Yang, *Adv. Mater.*, 2006, **18**, 2604–2608.
123 Y. Huang, X. Zhang, F. Zheng, S. Zou, M. Li, P. Huang and Y. Zeng, *Mater. Today Commun.*, 2022, **33**, 104304.
124 M. Mombrú Frutos, C. Grosso, Á. Olivera, H. Bentos Pereira, L. Fornaro and I. Aguiar, *Inorg. Chem.*, 2022, **61**, 9231–9241.
125 S. Sharma, D. Kumar and N. Khare, *Int. J. Hydrogen Energy*, 2019, **44**, 3538–3552.
126 X. Yang, J. Guo, Z. Y. Wang, W. H. Gu, Q. Shan, J. Feng and Z. H. Ge, *J. Alloys Compd.*, 2022, **922**, 166252.
127 M. Ye, F. Shi, M. Shen, W. Qin, C. Ren and Z. Yang, *Colloids Surf., A*, 2021, **613**, 126094.
128 T. Thongtem, A. Phuruangrat, S. Wannapop and S. Thongtem, *Mater. Lett.*, 2010, **64**, 122–124.
129 B. Roy, A. P. Chattopadhyay, A. Samadder and A. R. Khuda-Bukhsh, *J. Sol-Gel Sci. Technol.*, 2016, **77**, 446–452.
130 F. Chang, C. Yang, X. Wang, S. Zhao, J. Wang, W. Yang, F. Dong, G. Zhu and Y. Kong, *J. Cleaner Prod.*, 2022, **380**, 135167.
131 M. Y. Malca, H. Bao, T. Bastaille, N. K. Saadé, J. M. Kinsella, T. Friščić and A. Moores, *Chem. Mater.*, 2017, **29**, 7766–7773.
132 S. Boughdachi, Y. Azizian-Kalandaragh, Y. Badali and Ş. Altındal, *J. Mater. Sci.: Mater. Electron.*, 2017, **28**, 17948–17960.
133 Z. Y. Wang, J. Guo, Y. Wang, Y. X. Zhang, J. Feng and Z. H. Ge, *Small*, 2023, **12**, 2310306.
134 G. J. Lee, Y. C. Zheng and J. J. Wu, *Catal. Today*, 2018, **307**, 197–204.
135 Y. Long, Q. Han, Z. Yang, Y. Ai, S. Sun, Y. Wang, Q. Liang and M. Ding, *J. Mater. Chem. A*, 2018, **6**, 13005–13011.
136 M. Marks, H. S. Jeppesen and N. Lock, *ACS Appl. Mater. Interfaces*, 2022, **14**, 23496–23506.
137 J. Zhang, T. Shi, T. Liu, F. Gao, D. Cai, P. Liu, S. Yang and Y. Zhang, *Appl. Surf. Sci.*, 2024, **653**, 159346.
138 J. Henle, P. Simon, A. Frenzel, S. Scholz and S. Kaskel, *Chem. Mater.*, 2007, **19**, 366–373.
139 C. Wang, C. Shao, Y. Liu and L. Zhang, *Scr. Mater.*, 2008, **59**, 332–335.
140 Q. Fu, C. Zhu, X. Zhao, X. Wang, A. Chaturvedi, C. Zhu, X. Wang, Q. Zeng, J. Zhou, F. Liu, B. K. Tay, H. Zhang, S. J. Pennycook and Z. Liu, *Adv. Mater.*, 2019, **31**, 1804945.
141 W. Han, C. Li, S. Yang, P. Luo, F. Wang, X. Feng, K. Liu, K. Pei, Y. Li, H. Li, L. Li, Y. Gao and T. Zhai, *Small*, 2020, **16**, 2000228.
142 L. Wang, S. Guo, Y. Chen, M. Pan, E. H. Ang and Z. Yuan, *ChemPhotoChem*, 2020, **4**, 110–119.
143 L. Zhang, A. A. S. Gonçalves, B. Jiang and M. Jaroniec, *Nanoscale*, 2020, **12**, 8277–8284.
144 J. Yang, T. Xie, Q. Zhu, J. Wang, L. Xu and C. Liu, *J. Mater. Chem. C*, 2020, **8**, 2579–2588.
145 K. Zhan, J. Liang, S. Wang, J. Liu, K. Ren, X. Zheng, H. Luo, Y. Peng, X. Zou, X. Bo, J. Li and X. Yu, *Cryst. Growth Des.*, 2012, **12**, 793–803.
146 K. Ren, J. Liu, J. Liang, K. Zhang, X. Zheng, H. Luo, Y. Huang, P. Liu and X. Yu, *Dalton Trans.*, 2013, **42**, 9706–9712.
147 K. Wang, H. Qiao, J. Li and X. Qi, *Appl. Surf. Sci.*, 2021, **565**, 150444.
148 J. Dong, L. Zhang, K. Lau, Y. Shu, S. Wang, Z. Fu, Z. Wu, X. Liu, B. Sa, J. Pei, J. Zheng, H. Zhan and Q. Wang, *Small*, 2023, **11**, 2309595.
149 X. Yang, L. Qu, F. Gao, Y. Hu, H. Yu, Y. Wang, M. Cui, Y. Zhang, Z. Fu, Y. Huang, W. Feng, B. Li and P. Hu, *ACS Appl. Mater. Interfaces*, 2022, **14**, 7175–7183.
150 M. Q. Li, L. Y. Dang, G. G. Wang, F. Li, M. Han, Z. P. Wu, G. Z. Li, Z. Liu and J. C. Han, *Adv. Mater. Technol.*, 2020, **5**, 2000180.
151 Y. Sun, S. Ye, J. Zhang, J. Song, F. Zhou and J. Qu, *J. Mater. Chem. C*, 2020, **8**, 14711–14717.
152 M. Q. Li, L. Y. Dang, G. G. Wang, F. Li, M. Han, Z. P. Wu, G. Z. Li, Z. Liu and J. C. Han, *Adv. Mater. Technol.*, 2020, **5**, 2000180.
153 X. Tian, H. Luo, R. Wei, C. Zhu, Q. Guo, D. Yang, F. Wang, J. Li and J. Qiu, *Adv. Mater.*, 2018, **30**, 1801021.
154 L. Y. Dang, M. Liu, G. G. Wang, D. Q. Zhao, J. C. Han, J. Q. Zhu and Z. Liu, *Adv. Funct. Mater.*, 2022, **32**, 2201020.
155 C. Liu, C. Wang, M. Chen, H. Hu and Q. Zhang, *J. Environ. Chem. Eng.*, 2021, **9**, 106096.
156 C. C. Yu, H. Chang, A. C. Sun and J. W. Chiou, *Vacuum*, 2019, **169**, 108918.
157 X. Yang, X. Lian, S. Liu, G. Wang, C. Jiang, J. Tian, J. Chen and R. Wang, *J. Phys. D: Appl. Phys.*, 2013, **46**, 035103.
158 M. Camacho-López, M. Ballesteros-Balbuena, A. Esparza-García, M. Flores-Castañeda, S. Camacho-López and M. A. Camacho-López, *Mater. Chem. Phys.*, 2022, **291**, 126685.
159 H. Akazawa, *Ceram. Int.*, 2023, **49**, 9069–9089.
160 Z. He, J. A. Koza, Y. C. Liu, Q. Chen and J. A. Switzer, *RSC Adv.*, 2016, **6**, 96832–96836.
161 S. D. Cosham, M. S. Hill, G. A. Horley, A. L. Johnson, L. Jordan, K. C. Molloy and D. C. Stanton, *Inorg. Chem.*, 2014, **53**, 503–511.

162 S. J. A. Moniz, C. S. Blackman, C. J. Carmalt and G. Hyett, *J. Mater. Chem.*, 2010, **20**, 7881–7886.
163 Z. Sun, D. Oka and T. Fukumura, *Cryst. Growth Des.*, 2019, **19**, 7170–7174.
164 T. A. Gadhi, L. S. Gómez-Velázquez, M. Bizarro, A. Hernández-Gordillo, A. Tagliaferro and S. E. Rodil, *Thin Solid Films*, 2017, **638**, 119–126.
165 M. Hofmann, L. Rößner, M. Armbrüster and M. Mehring, *ChemistryOpen*, 2020, **9**, 277–284.
166 X. Yang, X. Lian, S. Liu, C. Jiang, J. Tian, G. Wang, J. Chen and R. Wang, *Appl. Surf. Sci.*, 2013, **282**, 538–543.
167 A. I. Alharthi, M. N. Shaddad, T. F. Qahtan, M. A. Alotaibi, A. A. Alanazi and P. Arunachalam, *J. Alloys Compd.*, 2023, **967**, 171733.
168 L. Peng, W. Lou, L. Li, Y. Zhang, X. Luo, N. Xu and J. Qiao, *Sep. Purif. Technol.*, 2024, **330**, 125372.
169 P. V. Shinde, B. G. Ghule, S. F. Shaikh, N. M. Shinde, S. S. Sangale, V. V. Jadhav, S. Y. Yoon, K. H. Kim and R. S. Mane, *J. Alloys Compd.*, 2019, **802**, 244–251.
170 G. Bandoli, D. Barreca, E. Brecacin, G. A. Rizzi and E. Tondello, *Chem. Vap. Deposition*, 1996, **2**, 238–242.
171 K. C. Chitrada, R. Gakhar, D. Chidambaram, E. Aston and K. S. Raja, *J. Electrochem. Soc.*, 2016, **163**, H546–H558.
172 M. Ahila, M. Malligavathy, E. Subramanian and D. P. Padiyan, *Solid State Ionics*, 2016, **298**, 23–34.
173 A. J. Maclachlan, F. T. F. O'Mahony, A. L. Sudlow, M. S. Hill, K. C. Molloy, J. Nelson and S. A. Haque, *ChemPhysChem*, 2014, **15**, 1019–1023.
174 S. Sharma and N. Khare, *Colloid Polym. Sci.*, 2018, **296**, 1479–1489.
175 M. A. Becker, J. G. Radich, B. A. Bunker and P. V. Kamat, *J. Phys. Chem. Lett.*, 2014, **5**, 1575–1582.
176 R. Nishikubo and A. Saeki, *J. Phys. Chem. Lett.*, 2018, **9**, 5392–5399.
177 S. S. Raut, J. A. Dhobale and B. R. Sankapal, *Phys. E*, 2017, **87**, 209–212.
178 K. A. Messalea, A. Zavabeti, M. Mohiuddin, N. Syed, A. Jannat, P. Atkin, T. Ahmed, S. Walia, C. F. McConville, K. Kalantar-Zadeh, N. Mahmood, K. Khoshmanesh and T. Daeneke, *Adv. Mater. Interfaces*, 2020, **7**, 2001131.
179 Y. C. Liang and T. H. Li, *Nanotechnol. Rev.*, 2021, **11**, 284–297.
180 O. C. Monteiro, T. Trindade, J. H. Park and P. O'Brien, *Chem. Vap. Deposition*, 2000, **6**, 230–232.
181 Y. Chen, B. Mei, H. Liu, Z. Sun and H. Zhang, *Cryst. Growth Des.*, 2022, **22**, 4203–4209.
182 F. Ding, Q. Wang, S. Zhou, G. Zhao, Y. Ye and R. Ghomashchi, *R. Soc. Open Sci.*, 2020, **7**, 200479.
183 S. Khan, S. Daemi, M. Kanwal, C. Xiao and F. E. Osterloh, *J. Mater. Chem. A*, 2023, **11**, 23418–23429.
184 B. Sun, T. Feng, J. Dong, X. Li, X. Liu, J. Wu and S. Ai, *CrystEngComm*, 2019, **21**, 1474–1481.
185 E. Chavez-Mendiola, M. C. Acosta-Enríquez, A. Carrillo-Castillo, O. Arellano-Tánori, J. O. Rivera-Nieblas and S. J. Castillo, *Chalcogenide Lett.*, 2018, **15**, 395–404.
186 Y. Wang, J. Chen, L. Jiang, K. Sun, F. Liu and Y. Lai, *J. Alloys Compd.*, 2016, **686**, 684–692.
187 M. Schuisky, *J. Electrochem. Soc.*, 1998, **145**, 4234–4239.
188 W. Zeng, L. P. Feng, J. Li, H. Pan, X. Zhang, X. Zheng, Y. Huang, R. Zhang and Z. Liu, *Chem. Mater.*, 2019, **31**, 9715–9720.
189 Z. Sun, Y. Wang and B. Mei, *J. Mater. Chem. C*, 2023, **11**, 3805–3811.
190 P. Liu, L. Yin, L. Feng, Y. Sun, H. Sun, W. Xiong, C. Xia, Z. Wang and Z. Liu, *Sci. China Mater.*, 2021, **64**, 189–197.
191 W. Han, C. Li, S. Yang, P. Luo, F. Wang, X. Feng, K. Liu, K. Pei, Y. Li, H. Li, L. Li, Y. Gao and T. Zhai, *Small*, 2020, **16**, 1–9.
192 T. Feeney, G. Aygur, T. Nguyen, S. Farooq, J. Mendes, H. Tuohey, D. E. Gómez, E. Della Gaspera and J. van Embden, *Nanotechnology*, 2023, **34**, 305404.
193 H. Jia, W. He, B. Zhang, L. Yao, X. Yang and Z. Zheng, *Appl. Surf. Sci.*, 2018, **441**, 832–840.
194 M. Wang, R. Quesada-Cabrera, S. Sathasivam, M. O. Blunt, J. Borowiec and C. J. Carmalt, *ACS Appl. Mater. Interfaces*, 2023, **15**, 49270–49280.
195 Z. Sun, S. Qin, D. Oka, H. Zhang, T. Fukumura, Y. Matsumoto and B. Mei, *Inorg. Chem.*, 2023, **62**, 8914–8922.
196 Z. Sun, B. Mei, H. Zhou, S. Qin and H. Zhang, *Ceram. Int.*, 2022, **48**, 25521–25527.
197 N. T. Hahn, S. Hoang, J. L. Self and C. B. Mullins, *ACS Nano*, 2012, **6**, 7712–7722.
198 Z. Sun, D. Oka and T. Fukumura, *Chem. Commun.*, 2020, **56**, 9481–9484.
199 S. J. Fang, P. Du, J. F. Zhang, C. H. Wang, Z. M. Xiao, B. Zhang, L. Cao, X. M. Fan and X. Ou, *Rare Met.*, 2022, **41**, 2567–2574.
200 Y. Song, Z. Li, H. Li, S. Tang, G. Mu, L. Xu, W. Peng, D. Shen, Y. Chen, X. Xie and M. Jiang, *Nanotechnology*, 2020, **31**, 165704.
201 Y. Liang, Y. Chen, Y. Sun, S. Xu, J. Wu, C. Tan, X. Xu, H. Yuan, L. Yang, Y. Chen, P. Gao, J. Guo and H. Peng, *Adv. Mater.*, 2019, **31**, 1901964.
202 Z. Wu, H. Yu, S. Shi and Y. Li, *J. Mater. Chem. A*, 2019, **7**, 14776–14789.
203 U. Khan, A. Nairan, K. Khan, S. Li, B. Liu and J. Gao, *Small*, 2023, **19**, 1–8.
204 M. Kang, H. B. Jeong, Y. Shim, H. J. Chai, Y. S. Kim, M. Choi, A. Ham, C. Park, M. K. Jo, T. S. Kim, H. Park, J. Lee, G. Noh, J. Y. Kwak, T. Eom, C. W. Lee, S. Y. Choi, J. M. Yuk, S. Song, H. Y. Jeong and K. Kang, *ACS Nano*, 2024, **18**, 819–828.
205 Z. Xing, J. Hu, M. Ma, H. Lin, Y. An, Z. Liu, Y. Zhang, J. Li and S. Yang, *J. Am. Chem. Soc.*, 2020, **141**, 19715–19727.
206 C. Tan, M. Tang, J. Wu, Y. Liu, T. Li, Y. Liang, B. Deng, Z. Tan, T. Tu, Y. Zhang, C. Liu, J. H. Chen, Y. Wang and H. Peng, *Nano Lett.*, 2019, **19**, 2148–2153.
207 J. Wu, C. Tan, Z. Tan, Y. Liu, J. Yin, W. Dang, M. Wang and H. Peng, *Nano Lett.*, 2017, **17**, 3021–3026.

208 W. Chen, U. Khan, S. Feng, B. Ding, X. Xu and B. Liu, *Adv. Funct. Mater.*, 2020, **30**, 2004960.
209 Q. Fu, C. Zhu, X. Zhao, X. Wang, A. Chaturvedi, C. Zhu, X. Wang, Q. Zeng, J. Zhou, F. Liu, B. K. Tay, H. Zhang, S. J. Pennycook and Z. Liu, *Adv. Mater.*, 2019, **31**, 1804945.
210 I. Bretos, R. Jiménez, J. Ricote and M. L. Calzada, *Chem. Soc. Rev.*, 2018, **47**, 291–308.
211 A. T. Hoang, K. Qu, X. Chen and J. H. Ahn, *Nanoscale*, 2021, **13**, 615–633.
212 C. Song, G. Noh, T. S. Kim, M. Kang, H. Song, A. Ham, M. K. Jo, S. Cho, H. J. Chai, S. R. Cho, K. Cho, J. Park, S. Song, I. Song, S. Bang, J. Y. Kwak and K. Kang, *ACS Nano*, 2020, **14**, 16266–16300.
213 W. X. Yu, B. Liu, W. Q. Huang, H. Zhou and S. Y. Xie, *J. Phys.: Condens. Matter*, 2023, **35**, 075401.
214 J. Zhou, L. Chen, Y. Wang, Y. He, X. Pan and E. Xie, *Nanoscale*, 2016, **8**, 50–73.
215 M. Kaur, P. Kumar and H. S. Ghotra, *Int. J. Hydrogen Energy*, 2024, **49**, 1095–1112.
216 G. Zhao, Z. Sun and B. Mei, *Adv. Opt. Mater.*, 2024, **12**, 1–10.
217 S. Ren, S. Gao, H. Lu, P. Rong, X. Zhang, L. Li, S. Jiao, D. Wang, Y. Zhang and J. Wang, *Appl. Surf. Sci.*, 2022, **590**, 153049.
218 W. Huang, C. Xing, Y. Wang, Z. Li, L. Wu, D. Ma, X. Dai, Y. Xiang, J. Li, D. Fan and H. Zhang, *Nanoscale*, 2018, **10**, 2404–2412.
219 G. Zhang, N. Zhao, K. Wang and J. Li, *Appl. Phys. A: Mater. Sci. Process.*, 2023, **129**, 411.
220 X. Yan, B. Shi, H. Cao, Z. Tian, C. Dai, W. Liu, Q. Yang and Y. Wang, *J. Mater. Chem. C*, 2023, **11**, 6928–6934.
221 P. Rong, S. Gao, M. Zhang, S. Ren, H. Lu, J. Jia, S. Jiao, Y. Zhang and J. Wang, *J. Alloys Compd.*, 2022, **928**, 167128.
222 J. Li, M. Wu, H. Zhang, S. Li, C. Wang, P. Wang, J. Sha and X. Zhou, *ACS Appl. Nano Mater.*, 2024, **7**, 594–605.
223 X. Y. Zhang, D. Wang, Z. Zeng, C. Zhao, Y. Liu, B. Zhang, J. Pan, D. Liu and J. Wang, *J. Sol. Energy Res. Updates*, 2022, **9**, 1–8.
224 S. Yang, S. Jiao, Y. Nie, H. Lu, S. Liu, Y. Zhao, S. Gao, D. Wang, J. Wang and Y. Li, *J. Mater. Chem. C*, 2022, **10**, 8364–8372.
225 G. Chen, Y. Zhou, G. Zhang, J. Li and X. Qi, *Ceram. Int.*, 2021, **47**, 25255–25263.
226 C. Lu, M. Luo, W. Dong, Y. Ge, T. Han, Y. Liu, X. Xue, N. Ma, Y. Huang, Y. Zhou and X. Xu, *Adv. Sci.*, 2023, **10**, 2205460.
227 J. Hui, *Appl. Phys. Express*, 2023, **16**, 015507.
228 B. Dong, X. Zhang, H. Cheng, X. Jiang and F. Wang, *Nanoscale*, 2023, **15**, 6333–6342.
229 H. Zhang, W. Luo, Z. Sun and C. Li, *Cryst. Growth Des.*, 2023, **23**, 2852–2859.
230 G. Zhao, Z. Sun and B. Mei, *Adv. Opt. Mater.*, 2024, **12**, 2302029.
231 S. Y. Jeong, K. S. Choi, H. M. Shin, T. L. Kim, J. Song, S. Yoon, H. W. Jang, M. H. Yoon, C. Jeon, J. Lee and S. Lee, *ACS Appl. Mater. Interfaces*, 2017, **9**, 505–512.
232 S. Majumder, M. Gu and K. H. Kim, *Mater. Sci. Semicond. Process.*, 2022, **141**, 106439.
233 M. Karimi Sahnesarayi, H. Sarpoolaky and S. Rastegari, *Int. J. Hydrogen Energy*, 2022, **47**, 7214–7227.
234 K. C. Chitrada, K. S. Raja, R. Gakhar and D. Chidambaram, *J. Electrochem. Soc.*, 2015, **162**, H380–H391.
235 P. Hajra, S. Shyamal, H. Mandal, P. Fageria, S. Pande and C. Bhattacharya, *Electrochim. Acta*, 2014, **123**, 494–500.
236 S. A. Patil, Y. T. Hwang, V. V. Jadhav, K. H. Kim and H. S. Kim, *J. Photochem. Photobiol., A*, 2017, **332**, 174–181.
237 Y. Wang, J. Chen, L. Jiang, K. Sun, F. Liu and Y. Lai, *J. Alloys Compd.*, 2016, **686**, 684–692.
238 B. Li, L. Shao, B. Zhang, R. Wang, M. Zhu and X. Gu, *J. Colloid Interface Sci.*, 2017, **505**, 653–663.
239 M. E. Kazyrevich, E. A. Streltsov, V. Malashchonak, A. V. Mazanik, A. I. Kulak, P. Ščajev and V. Grivickas, *Electrochim. Acta*, 2018, **290**, 63–71.
240 Y. Ling, Y. Dai and J. Zhou, *J. Colloid Interface Sci.*, 2020, **578**, 326–337.
241 L. W. Shan, L. Q. He, J. Suriyaprakash and L. X. Yang, *J. Alloys Compd.*, 2016, **665**, 158–164.
242 S. Cui, G. Shan and L. Zhu, *Appl. Catal., B*, 2017, **219**, 249–258.
243 L. Jiang, J. Li, Y. Li, X. Wu and G. Zhang, *Appl. Catal., B*, 2021, **294**, 120249.
244 V. Andrei, R. A. Jagt, M. Rahaman, L. Lari, V. K. Lazarov, J. L. MacManus-Driscoll, R. L. Z. Hoye and E. Reisner, *Nat. Mater.*, 2022, **21**, 864–868.
245 S. K. Poznyak and A. I. Kulak, *Electrochim. Acta*, 1990, **35**, 1941–1947.
246 Q. Gao, Z. Shao, S. Sun, H. Guan, X. Gao, N. Zhang, J. Yao, F. Gao and W. Feng, *Adv. Opt. Mater.*, 2024, 2302658.
247 J. Zhang, T. Lin, L. Si, A. Wang, Q. He, H. Ye, J. Lu, Q. Wang, Z. Liang, F. Jin, S. Chen, M. Fan, E.-J. Guo, Q. Zhang, L. Gu, Z. Luo, W. Wu and L. Wang, *Science*, 2024, **383**, 388–394.
248 R. Xu, J. Huang, E. S. Barnard, S. S. Hong, P. Singh, E. K. Wong, T. Jansen, V. Harbola, J. Xiao, B. Y. Wang, S. Crossley, D. Lu, S. Liu and H. Y. Hwang, *Nat. Commun.*, 2020, **11**, 3141.
249 X. Hao, T. Huang, M. Li, Y. Pan, L. Liao, K. Zhang and A. Qin, *J. Mater. Chem. A*, 2023, **11**, 16403–16413.
250 A. K. Singh and D. Sarkar, *Nanoscale*, 2018, **10**, 13130–13139.
251 A. Zhao, L. Zhang, Y. Guo, H. Li, S. Ruan and Y. J. Zeng, *2D Mater.*, 2020, **8**, 012004.
252 G. Zhao, B. Mei, Y. Chen and Z. Sun, *Inorg. Chem.*, 2024, **63**, 3460–3466.
253 H. Sun, G. Yang, J. Chen, C. Kirk and N. Robertson, *J. Mater. Chem. C*, 2020, **8**, 13253–13262.
254 S. Li, L. Xu, X. Kong, T. Kusunose, N. Tsurumachi and Q. Feng, *J. Mater. Chem. C*, 2020, **8**, 3821–3829.
255 S. Li, L. Xu, X. Kong, T. Kusunose, N. Tsurumachi and Q. Feng, *Phys. Rev. Appl.*, 2021, **15**, 034040.
256 L. Xu, Y. Zhang, B. Liu, X. Wang, G. Zhu, L. Wang, S. Wang and W. Huang, *Nano Res.*, 2024, **17**, 1140–1150.

